

Aromatase is a cytochrome P450 enzyme that plays a crucial role in the estrogen biosynthesis (1). It catalyzes the conversion of Δ^4 -androstendione into estrone and that of testosterone (T) into estradiol (E_2) in the placenta and ovary as well as in other tissues such as the fat, skin, bone, and brain (1). It is encoded by *CYP19A1* consisting of at least 11 noncoding exons 1 and nine coding exons 2–10 (Supplemental Fig. 1, published on The Endocrine Society's Journals Online web site at <http://jcem.endojournals.org>) (2, 3). Each exon 1 is accompanied by a tissue-specific promoter and is spliced alternatively onto a common splice acceptor site at exon 2, although some transcripts are known to contain two of the exons 1, probably due to a splice error (2, 4). Of the 11 exons 1, exon 1.4 appears to play a critical role in the regulation of estrogen biosynthesis in males because this exon contains a major promoter for extragonadal tissues including the skin and fat (2).

Excessive *CYP19A1* expression causes a rare autosomal dominant disorder known as aromatase excess syndrome (AEXS) (5–8). AEXS is characterized by pre- or peripubertal onset gynecomastia, advanced bone age from childhood to the pubertal period, and short adult height in affected males (5–8). Affected females may show several clinical features such as macromastia, precocious puberty, irregular menses, and short adult height (6–8). In this regard, previous studies have identified four heterozygous cryptic inversions around *CYP19A1* in patients with AEXS (5, 8). Each inversion results in the formation of a chimeric gene consisting of a noncoding exon(s) of a neighboring gene (*CGNL1*, *MAPK6*, *TMOD3*, or *TLN2*) and coding exons of *CYP19A1*. Because this condition is predicted to cause aberrant *CYP19A1* expression in tissues in which each neighboring gene is expressed, such inversions have been regarded to be responsible for AEXS (5, 8).

However, such inversions have been revealed only in a few patients with AEXS, and, despite extensive studies, no other underlying genetic mechanisms have been identified to date (6, 8–10). Here we report novel genomic rearrangements in AEXS and discuss primary phenotypic determining factors in AEXS.

Patients and Methods

Patients

This study was approved by the Institutional Review Board Committee at the National Center for Child Health and Development and was performed after obtaining informed consent. We examined 18 male patients aged 8–69 yr (cases 1–18) from six unrelated families A–F (Fig. 1A). The probands were ascertained by bilateral gynecomastia (Fig. 1B) and the remaining 12 males by familial studies. Ten other males allegedly had gynecomastia. There were four obligatory carrier females.

Phenotypic assessment showed pre- or peripubertal onset gynecomastia in all cases, small testes and fairly preserved masculinization in most cases, obvious or relative tall stature in childhood and grossly normal or relative short stature in adulthood, and age-appropriate or mildly advanced bone ages (Table 1) (for detailed actual data, see Supplemental Table 1). Such clinical features, especially gynecomastia, tended to be milder in cases 1–4 from families A and B than in the remaining cases from families C–F. Fertility or spermatogenesis was preserved in all adult cases (≥ 20 yr). In addition, the obligatory carrier females from families B and D had apparently normal phenotype, and such females from families E and F exhibited early menarche (9.0 yr) and short adult stature (-2.8 SD), respectively.

Blood endocrine studies revealed that LH values were grossly normal at the baseline and variably responded to GnRH stimulation, whereas FSH values were low at the baseline and responded poorly to GnRH stimulation, even after preceding GnRH priming (Table 1) (for detailed actual data, see Supplemental Table 1) (see also Fig. 1C for the cases aged ≥ 15 yr). Δ^4 -Androstendione, T, and dihydrotestosterone values were low or normal. A human chorionic gonadotropin (hCG) test indicated relatively low but normal T responses in five young cases. In most cases, estrone values were elevated, E_2 values were normal or elevated, and E_2/T ratios were elevated. These endocrine data were grossly similar among cases 1–18.

Aromatase inhibitor (anastrozole, 1 mg/d) was effective in all the four cases treated (Supplemental Table 1) (see also Fig. 1C for cases aged ≥ 15 yr). Gynecomastia was mitigated within 6 months of treatment, and endocrine data were ameliorated within 1 month of treatment.

Primers

Primers used in this study are shown in Supplemental Table 2.

CYP19A1 mRNA levels and aromatase activities

We analyzed relative mRNA levels of *CYP19A1* and catalytic activities of aromatase in skin fibroblasts (SF) and lymphoblastoid cell lines (LCL). mRNA were extracted by a standard method and were subjected to RT-PCR using a high capacity RNA-to-cDNA kit (Life Technologies, Carlsbad, CA). A relative amount of *CYP19A1* mRNA against *B2M* was determined by the real-time PCR method using the Taqman gene expression assay on ABI PRISM 7500fast (Life Technologies) (assay no. Hs00903411_m1 for *CYP19A1* and Hs99999907_m1 for *B2M*). PCR was performed in triplicate. Aromatase activity was determined by a tritium incorporation assay (11). In brief, the samples were incubated with androstenedione-2- 3 H for 2 h, and 3 HH₂O in the supernatant of the culture media was measured with a scintillation counter LSC-5100 (Aloka, Tokyo, Japan).

Sequence analysis of CYP19A1

Leukocyte or SF genomic DNA samples from the six probands and additional four male patients (Fig. 1A) were PCR amplified for the coding exons 2–10 and their flanking splice sites of *CYP19A1*. Subsequently the PCR products were subjected to direct sequencing from both directions on CEQ 8000 autosequencer (Beckman Coulter, Fullerton, CA).

Genome structure analysis

Oligonucleotide array-based comparative genomic hybridization (CGH) analyses were carried out using a custom-built

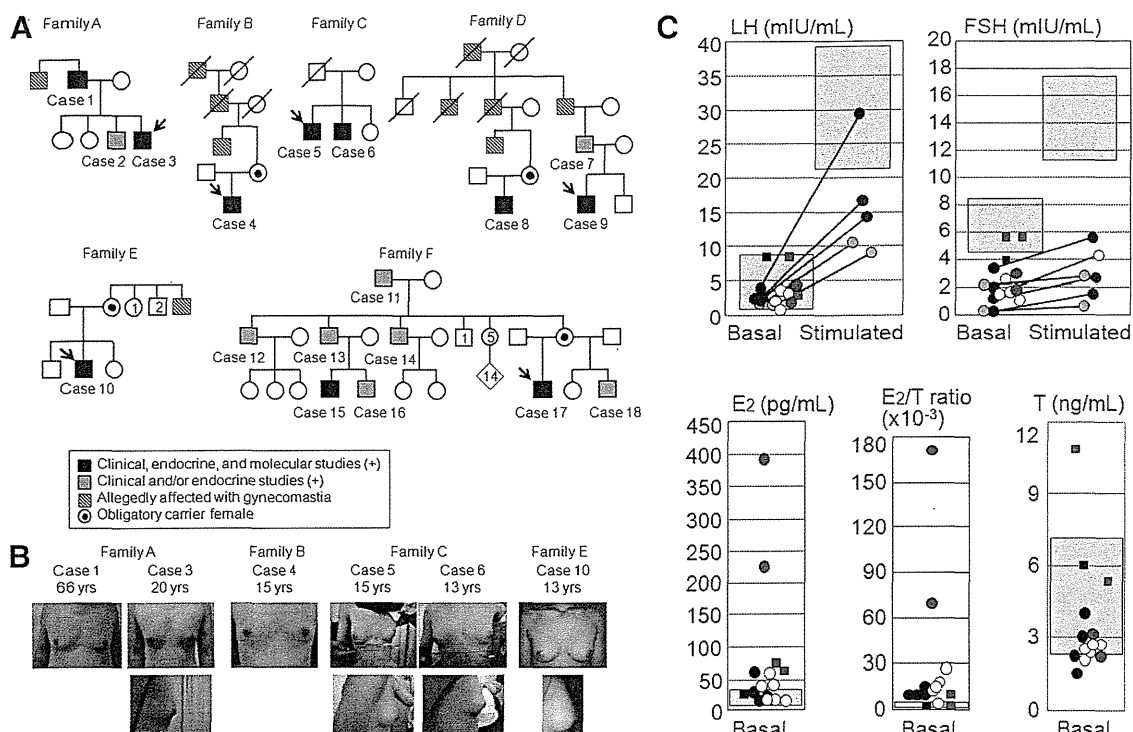


FIG. 1. Summary of clinical data. **A**, Pedigrees of six families with patients exhibiting AEXS-compatible phenotype. Families A–E are of Japanese origin, and family F is of German origin. Cases from families A–D were hitherto unreported, whereas those from families E and F have previously been described as having AEXS phenotypes (6, 8). **B**, Gynecomastia of six cases. **C**, Endocrine data in cases 15 yr of age or older. The black, white, and red colors represent the data in cases of the duplication, the deletion, and the inversion types, respectively; the blue color indicates the data of GnRH test after GnRH priming in two cases of the duplication type. The data at the time of diagnosis are denoted by circles, and those on aromatase inhibitor (anastrozole) treatment (1 mg/d in the duplication and the deletion types and 2–4 mg/d in the inversion types) are depicted by squares. The light purple areas represent the normal reference ranges.

oligo-microarray containing 90,000 probes for the 15q11.2-q26.3 region and approximately 10,000 reference probes for other chromosomal region (2 × 105K format, design identification 026533) (Agilent Technologies, Palo Alto, CA). The procedure was as described in the manufacturer's instructions. Fluorescence *in situ* hybridization (FISH) analysis was performed for lymphocyte or SF metaphase spreads, using long PCR products (FISH probes 1 and 2) for rearranged regions and CEP 15 probe for *D15Z4* used as an internal control (Abbott, Abbott Park, IL). The FISH probes 1 and 2 were labeled with digoxigenin and detected by rhodamine antidigoxigenin, and the CEP 15 probe was detected according to the manufacturer's protocol.

Characterization of the duplications and deletions

The duplication junctions were determined by direct sequencing for standard PCR products obtained with a variety of combinations of primers hybridizing to different positions within the *CYP19A1* exons 1 region. The deletion junctions were identified by direct sequencing of the long PCR products obtained with primer pairs flanking the deletions. The sizes of duplications and the deletions were determined by comparing obtained sequences with NT_010194 sequences at the National Center for Biotechnology Information Database (<http://www.ncbi.nlm.nih.gov/>; Bethesda, MD). The presence or absence of repeat sequences around the breakpoints was examined with Repeatmasker (<http://www.repeatmasker.org>).

For mRNA analysis, we performed 5'-rapid amplification of cDNA ends (RACE) using a SMARTER RACE cDNA amplifi-

cation kit (Takara Bio, Ohtsu, Japan). For both duplications and deletions, first PCR was carried out using the forward primer mix provided in the kit (Universal primer A mix) and an antisense reverse primer specific to *CYP19A1* exon 3 (RACE Rev). Second PCR was carried out for diluted products of the first PCR, using the nested forward primer of the kit (Nested universal primer A) and a reverse primer for *CYP19A1* exon 2 (Nested Rev). For duplications, furthermore, second PCR was also performed using various combinations of primers hybridizing to each *CYP19A1* exon 1. Subsequently PCR products were subcloned into TOPO cloning vector (Life Technologies) and subjected to direct sequencing. Then, the obtained sequences were examined with BLAST Search (National Center for Biotechnology Information). The presence or absence of promoter-compatible sequences was analyzed with the University of California, Santa Cruz, genome browser (<http://genome.ucsc.edu/>).

Relative mRNA levels of *CYP19A1* and its neighboring genes

We investigated relative mRNA levels of *CYP19A1* and *DMXL2* as well as those of *CGNL1*, *MAPK6*, *TMOD3*, and *TLN2* involved in the previously reported cryptic inversions (5, 8) in various human tissues. In this experiment, cDNA of SF and LCL were obtained from control males, and the remaining human cDNA samples were purchased from Life Technologies or Takara Bio. Relative quantification of mRNA against *TBP* was carried out using Taqman gene expression assay kit

TABLE 1. Summary of clinical studies in male patients with aromatase excess syndrome^a

	Present study						Previous studies			
	Family A	Family B	Family C	Family D	Family E	Family F	Family 1	Family 2	Sporadic	
Cases	Cases 1–3	Case 4	Cases 5–6	Cases 7–9	Case 10	Cases 11–18	Two cases ^b	Proband ^c	Patient 1	Patient 2
Mutation type	Duplication	Duplication	Deletion	Deletion	Deletion	Deletion	Inversion	Inversion	Inversion	Inversion
Phenotypic findings										
Gynecomastia	Yes (mild)	Yes (mild)	Yes (moderate)	Yes (moderate)	Yes (moderate)	Yes (moderate)	Yes (severe)	Yes (severe)	Yes (severe)	Yes (severe)
Pubertal defect	Yes (mild)	Yes (mild)	Yes (mild)	No	No	Yes (mild)	N.D.	Yes (mild)	No	N.D.
Short adult height	No	No	N.D.	No	N.D.	No	Yes	N.D.	Yes	N.D.
Spermatogenesis	Preserved	N.D.	N.D.	Preserved	N.D.	Preserved	N.D.	N.D.	N.D.	N.D.
Endocrine findings										
LH (basal)	Normal	Normal	Normal	Normal/low	Normal	Normal/low	Normal	Normal/low	Normal	N.E.
LH (GnRH stimulated) ^d	Low	Normal	High	Normal	Normal	Normal	N.E.	Low	N.E.	N.E.
FSH (basal)	Low	Low	Low	Low	Low	Normal/low	Normal/low	Low	Low	N.E.
FSH (GnRH stimulated) ^d	Low	Low	Low	Low	Low	Low	N.E.	Low	N.E.	N.E.
T (basal)	Normal/low	Normal	Normal/low	Normal/low	Normal	Normal/low	Normal	Normal/low	Low	N.E.
T (hCG stimulated) ^e	N.E.	N.E.	Normal	Normal	Normal	Normal	N.E.	Normal	Low	N.E.
E ₁ (basal)	High	High	N.E.	High	High	High	High	High	High	N.E.
E ₂ (basal)	Normal	High	High	Normal	High	Normal/high	High	High	High	N.E.
E ₂ to T ratio	High	High	High	High	High	High	High	High	High	N.E.

E₁, Estrone; N.D., not determined; N.E., not examined.

^a Detailed actual data are shown in Supplemental Table 1.

^b A father-son pair.

^c The sister has macromastia, large uterus, and irregular menses; the parental phenotype has not been described.

^d GnRH 100 µg/m² (maximum 100 µg) bolus iv; blood sampling at 0, 30, 60, 90, and 120 min.

^e hCG 3000 IU/m² (maximum 5000 IU) im for 3 consecutive days; blood sampling on d 1 and 4.

(assay no. Hs00903411_m1 for CYP19A1; Hs00324048_m1 for DMXL2; Hs00262671_m1 for CGNL1; Hs00833126_g1 for MAPK6; Hs00205710_m1 for TMOD3; Hs00322257_m1 for TLN2; and Hs99999910_m1 for TBP). The experiments were carried out three times.

3A). FISH analysis supported the duplications and confirmed the deletions.

Characterization of the cryptic duplications

Aberrant PCR products were obtained with the P2 primer (which amplifies a segment between exon I.1 and exon IIa with the P1 primer) and the P3 primer (which amplifies a segment between exon I.2 and exon I.6 with the P4 primer), and sequencing of the PCR products showed the same tandem duplication involving seven of the 11 exons 1 of CYP19A1 in cases from families A and B (Fig. 3B). The duplicated region was 79,156-bp long, and the

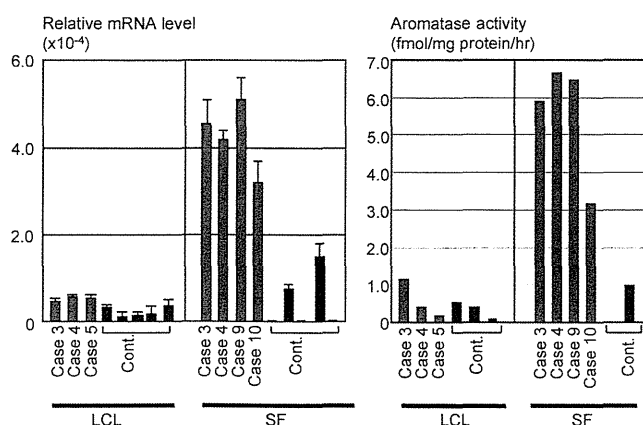


FIG. 2. Relative CYP19A1 mRNA levels against B2M and catalytic activities of aromatase.

Results

CYP19A1 mRNA levels and aromatase activities

Although relative mRNA levels of CYP19A1 and catalytic activities of aromatase were grossly similar between LCL of case 3 (family A), case 4 (family B), and case 5 (family C) and those of control subjects, they were significantly higher in SF of case 3 (family A), case 4 (family B), case 9 (family D), and case 10 (family E) than in those of control subjects (Fig. 2).

Sequence analysis of CYP19A1

Direct sequencing showed no mutation in CYP19A1 coding exons 2–10 of the 10 cases examined.

Genome structure analysis

CGH analysis revealed heterozygous cryptic duplications involving most of the CYP19A1 exons 1 region in cases from families A and B, heterozygous cryptic deletions involving most of DMXL2 and part of GLDN in cases from family C, and heterozygous cryptic deletions involving most of DMXL2 in cases from families D–F (Fig.

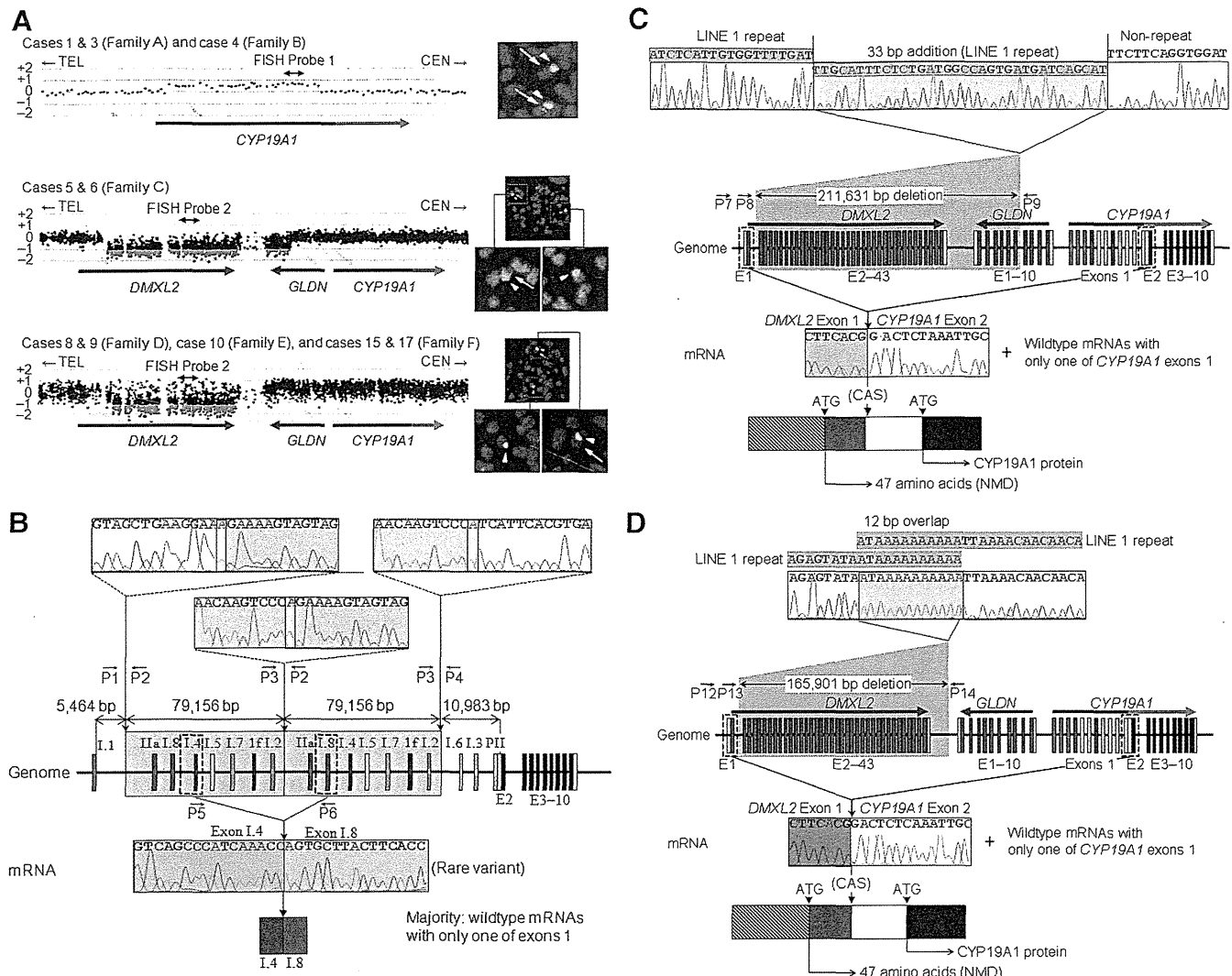


FIG. 3. Summary of molecular studies. For *CYP19A1*, the dark and light blue lines represent the genomic regions for noncoding exons 1 and coding exons 2–10, respectively. **A**, Oligoarray CGH and FISH analyses. In CGH analysis, the black, red, and green dots denote signals indicative of the normal, the increased ($>+0.5$), and the decreased (<-1.0) copy numbers, respectively. In FISH analysis, two red signals with an apparently different density are identified in cases from families A and B by FISH probe 1, whereas only a single red signal is found in cases from families C–F by FISH probe 2. The green signals are derived from the internal control probe. **B**, Schematic representation of the tandem duplication shared in common by cases 1 and 3 from family A and case 4 from family B. Genome, The junction sequence of the tandem duplication (yellow boxes) is shown, together with the original normal sequences at the 5'- and the 3'-ends of the duplicated region. The sequences highlighted with light green and light orange are identical, and 1 bp (A) is shared at the junction point (highlighted with light yellow). mRNA, The sequence of a rare clone is shown. The 3'-end of exon I.4 is connected with the 5'-end of exon I.8. **C**, Schematic representation of the deletion in sibling cases 5 and 6 from family C. Genome, The junction sequence of the deletion (a gray area) is shown. The fusion has occurred between a LINE 1 repeat sequence (highlighted with blue) at intron 1 of *DMXL2* and a nonrepeat sequence at intron 4 of *GLDN* and is accompanied by an addition of a 33-bp segment with a LINE 1 repeat sequence. mRNA, The sequence of a rare chimeric gene transcript is shown. *DMXL2* exon 1 consisting of a noncoding region (a red striped box) and a coding region (a red box) is spliced onto the common acceptor site (CAS) of *CYP19A1* exon 2 comprising an untranslated region (a white box) and a coding region (a black box). Thus, this transcript has two translation initiation codons (ATG), although the mRNA destined to produce a 47-amino acid protein from the ATG on *DMXL2* exon 1 is predicted to undergo NMD. **D**, Schematic representation of the deletion shared in common by cases 8 and 9 from family D, case 10 from family E, and cases 15 and 17 from family F. Genome, The junction sequence of the deletion (a gray area) is shown. The fusion has occurred between a LINE 1 repeat sequence (highlighted with blue) at intron 1 of *DMXL2* and that at a downstream region of *DMXL2*, with an overlap of a 12-bp segment. mRNA, The sequence of a chimeric gene transcript is delineated. The mRNA structure is the same as that described in the legend for Fig. 3C.

fusion occurred between nonrepeat elements with an overlap of one nucleotide.

All the 5'-RACE products (>500 clones) obtained from LCL and SF of case 3 (family A) and case 4 (family B) were found to be associated with a single exon 1, as observed in

control materials. However, PCR amplifications for the 5'-RACE products with a variety of combinations of primers hybridizing to each exon 1 and subsequent sequencing of the PCR products revealed the presence of a chimeric clone consisting of exon I.4 at the 5' side and exon I.8 at

the 3' side in both LCL and SF (Fig. 3B). Although such a chimeric clone would have been produced by a splice error, this indicated that duplicated exon 1.4 at the distal nonphysiological position functioned as a transcription start site.

Characterization of the cryptic deletions

In cases from family C, long PCR products were obtained with the P7 primer and the P9 primer, and the deletion junction was determined by direct sequencing with the P8 primer (Fig. 3C). The deleted region was 211,631-bp long and involved exons 2–43 of *DMXL2* and exons 5–10 of *GLDN*. The two breakpoints resided within a LINE 1 repeat sequence and a nonrepeat sequence respectively, and a 33-bp segment with a LINE 1 repeat sequence was inserted to the fusion point. In cases from families D–F, long PCR products were obtained by sequential amplifications with the P12 primer and the P14 primer and with the P13 primer and the P14 primer, and an identical deletion was identified by direct sequencing with the P13 primer (Fig. 3D). The deletion was 165,901-bp long and involved exons 2–43 of *DMXL2*. The fusion occurred between two LINE 1 repeat sequences with an overlap of a 12-bp segment.

Sequence analysis of the 5'-RACE products obtained from LCL of cases 5 and 6 (family C) and from SF of case 9 (family D) and case 10 (family E) revealed the presence of a few clones with *DMXL2* exon 1 (2–5%), together with multiple clones with a single wild-type *CYP19A1* exon 1 (Fig. 3, C and D). Such a chimeric mRNA clone was absent from control materials. Furthermore, *DMXL2* exon 1 was found to be accompanied by a promoter-compatible sequence (Supplemental Fig. 2). This indicated a cryptic usage of *DMXL2* exon 1 as an alternative *CYP19A1* transcription start site in cases with deletions. Notably, because of the presence of the translation start codon on *DMXL2* exon 1, mRNAs of the *DMXL2/CYP19A1* chimeric genes are predicted to produce two proteins, *i.e.* *CYP19A1* protein and an apparently nonfunctional 47-amino acid protein with a termination codon on *CYP19A1* exon 2, when the translation started from the initiation codons on *CYP19A1* exon 2 and on *DMXL2* exon 1, respectively. Furthermore, mRNA destined to yield the 47-amino acid protein is predicted to undergo nonsense-mediated mRNA decay (NMD) because it satisfies the condition for the occurrence of NMD (12).

Relative mRNA levels of *CYP19A1* and its neighboring genes

CYP19A1 showed a markedly high expression in the placenta and a relatively weak expression in a limited number of tissues including hypothalamus and ovary. By

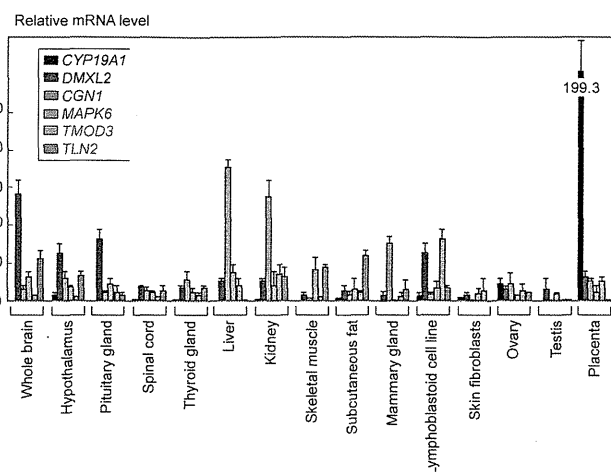


FIG. 4. Expression patterns of *CYP19A1* and the five neighboring genes involved in the chimeric gene formation. Relative mRNA levels against *TBP* are shown.

contrast, *DMXL2* was expressed in a range of tissues with some degree of variation as well as *CGNL1*, *MAPK6*, *TMOD3*, and *TLN2* (Fig. 4).

Discussion

We identified cryptic duplications of the *CYP19A1* promoter region and deletions of the *CYP19A1* upstream region in cases with AEXS. The tandem duplications would have caused *CYP19A1* overexpression because of an increased number of the wild-type transcription start sites. Indeed, because a rare mRNA variant with exon I.4 and exon I.8 was identified, this implies that duplicated exons 1 at the distal nonphysiological position can also function as transcription start sites. Similarly, the deletions would have caused *CYP19A1* overexpression because of a cryptic usage of *DMXL2* exon 1 with a putative promoter function as an extra transcription start site for *CYP19A1*. Indeed, because a few clones with *DMXL2* exon 1 and *CYP19A1* exon 2 were identified, this confirms the formation of a *DMXL2/CYP19A1* chimeric gene. Thus, our results suggest for the first time that duplications of a physiological promoter and deletions of an upstream region can cause overexpression of a corresponding gene and resultant human genetic disease.

Such cryptic genomic rearrangements can be generated by several mechanisms. The tandem duplication in families A and B would be formed by a replication-based mechanism of fork stalling and template switching that occurs in the absence of repeat sequences and is associated with microhomology (13). The deletion in family C is explained by nonhomologous end joining that takes place between nonhomologous sequences and is frequently accompanied by an insertion of a short segment at the fusion point (13).

The deletion in families D–F is compatible with a repeat sequence mediated nonallelic intrachromosomal or interchromosomal recombination (13). Thus, in conjunction with the previously identified four cryptic inversions that are also explainable by fork stalling and template switching or nonallelic recombination (8), genomic sequence around *CYP19A1* appears to harbor particular motifs that are vulnerable to replication and recombination errors.

To date, three types of cryptic genomic rearrangements have been identified in patients with AEXS, *i.e.* duplication type, deletion type (two subtypes), and inversion type (four subtypes) (Fig. 5). Here, although the deletion and the inversion types are associated with heterozygous impairment of neighboring genes (deletion or disconnection between noncoding exon(s) and coding exons), the phenotypes of patients are well explained by excess-

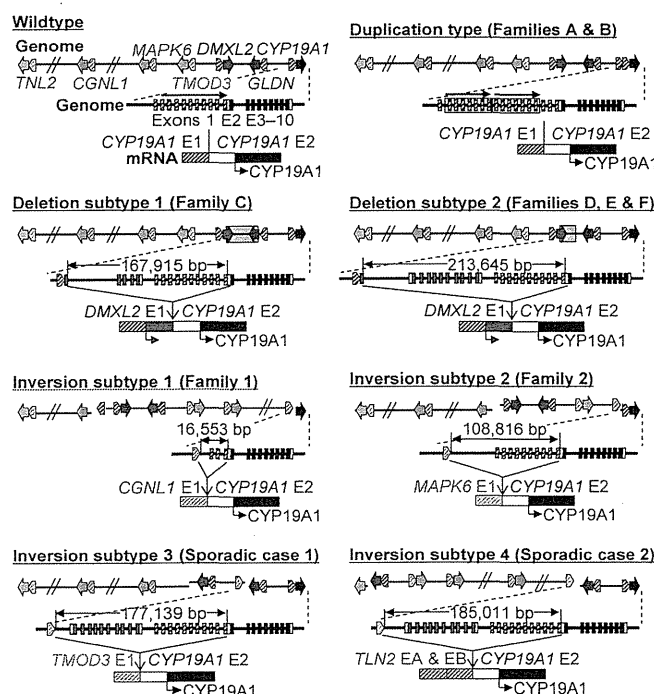


FIG. 5. Schematic representation of the rearranged genome and mRNA structures. The white and black boxes of *CYP19A1* exon 2 show untranslated region and coding region, respectively (for details, see Supplemental Fig. 1). For the duplication type and the deletion subtypes, see Fig. 3, C and D, for details. For genome, the striped and painted arrows indicate noncoding and coding exons, respectively (5'→3'). The inverted genomic regions are delineated in blue lines. For mRNA, colored striped boxes represent noncoding regions of each gene. For *TLN2*, exons A and B correspond to the previously reported exons 1 and 2 (8); because current exon 1 in the public database indicates the first coding exon, we have coined the terms exons A and B for the noncoding exons. The deletion and inversion types are associated with heterozygous impairment of neighboring genes [deletion or disconnection between noncoding exon(s) and the following coding exons]. The inversion subtype 1 is accompanied by inversion of eight of the 11 *CYP19A1* exons 1, and the inversion subtype 2 is associated with inversion of the placenta-specific *CYP19A1* exon I.1.

sive *CYP19A1* activity alone. Thus, haploinsufficiency of these neighboring genes would not have a major clinical effect.

For the deletion and inversion types, two factors should be considered. One factor is expression patterns of each chimeric gene. In this regard, the five genes involved in the formation of chimeric genes are widely expressed, with some degree of variation (Fig. 4). Furthermore, *in silico* analysis revealed promoter-compatible sequences around exon 1 of *DMXL2*, *CGNL1*, *MAPK6*, and *TMOD3* in multiple cell types, although such sequences remain to be identified for noncoding exons of *TLN2* (Supplemental Fig. 2). These findings imply that the chimeric genes show wide expression patterns because expression patterns of chimeric genes would follow those of the original genes.

The other factor is expression dosage of each chimeric gene. In this context, the *DMXL2/CYP19A1* chimeric mRNA was identified only in 2–5% of transcripts from SF, whereas the *CGNL1/CYP19A1* chimeric mRNA and the *TMOD3/CYP19A1* chimeric mRNA accounted for 89–100% and 80% of transcripts from SF, respectively (no data for the *MAPK6/CYP19A1* and the *TLN2/CYP19A1* chimeric genes) (5). This difference is obviously inexplicable by the relative expression level in SF that is grossly similar between *DMXL2* and *TMOD3* and is quite low for *CGNL1* (Fig. 4). In this regard, it is notable that a translation start codon and a following coding region are present on exon 1 of *DMXL2* (Fig. 5). It is likely that *DMXL2/CYP19A1* chimeric mRNA transcribed by the *DMXL2* promoter preferentially recognized the natural start codon on *DMXL2* exon 1 and underwent NMD and that rather exceptional chimeric mRNAs, which recognized the start codon on *CYP19A1* exon 2, were identified by 5'-RACE. By contrast, such a phenomenon would not be postulated for the inversion-mediated chimeric mRNA because of the absence of a translation start codon on the fused exon 1 of *CGNL1* and *TMOD3* (as well as exon 1 of *MAPK6* and exons A and B of *TLN2*) (Fig. 5). For the *CGNL1/CYP19A1* chimeric gene, furthermore, the physical distance between *CGNL1* exon 1 and *CYP19A1* exon 2 is short, and whereas a splice competition may be possible between exon 1 of neighboring genes and original *CYP19A1* exons 1, eight of 11 *CYP19A1* exons 1 including exon I.4 functioning as the major promoter in SF have been disconnected from *CYP19A1*-coding exons by inversion. These structural characters would have also contributed to the efficient splicing between *CGNL1* exon 1 and *CYP19A1* exon 2 (14). In this context, although the *CGNL1/CYP19A1* chimeric gene is associated with functional loss of eight *CYP19A1* exons 1 and the resultant reduction of *CYP19A1* expression in *CYP19A1*-expressing tissues, overall aromatase activity would be increased

by the wide expression of the chimeric gene. These structural properties would primarily explain the difference in the expression dosage of chimeric mRNA between the deletion and the inversion types.

It is inferred, therefore, that the duplication type simply increases *CYP19A1* transcription in native *CYP19A1*-expressing tissues, whereas the deletion and the inversion types cause relatively mild and severe *CYP19A1* overexpression in a range of tissues, respectively. These notions would grossly explain why clinical features of affected males and carrier females and endocrine profiles of affected males are apparently milder in the duplication and the deletion types than in the inversion type and why clinical findings were ameliorated with 1 mg/d of anastrozole in the duplication and the deletion types and with 2–4 mg/d of anastrozole in the inversion type. In addition, the different expression pattern between *CYP19A1* and *DMXL2* may explain, in terms of autocrine and/or paracrine effects, why phenotypic features such as gynecomastia tended to be more severe in the deletion type than in the duplication type under similar endocrine profiles.

Furthermore, several findings are notable in this study. First, a similar degree of FSH-dominant hypogonadotropic hypogonadism is present in the three types, with no amelioration of FSH responses to GnRH stimulation after GnRH priming in two cases with the duplication. This suggests that a relatively mild excess of circulatory estrogens, as observed in the duplication and the deletion types, can exert a strong negative feedback effect on FSH secretion, primarily at the pituitary, as has been suggested previously (15–19). Second, although basal T values appear to be mildly and similarly compromised in the three types, age-matched comparison suggests that T responses to hCG stimulation are apparently normal in the duplication and the deletion types and somewhat low in the inversion type. These data, although they remain fragmentary, would primarily be compatible with fairly preserved LH secretion in the three types and markedly increased estrogen values in the inversion type because T production is under the control of LH (1), and excessive estrogens compromise testicular steroidogenic enzyme activity (20, 21). Lastly, although testis volume appears somewhat small, fertility (spermatogenesis) is normally preserved in the three types. This would be consistent with the FSH-dominant hypogonadotropic hypogonadism because FSH plays only a minor role in male fertility (spermatogenesis) (22). Indeed, males with mutations of *FSHR* encoding FSH receptor as well as mice lacking *FSHB* or *FSHR* can be fertile (23, 24).

The results of this study are contrastive to those of the previous studies. In the previous studies, inversions only have been identified, and each inversion is specific to each

family or patient (8). By contrast, in this study, the identical duplication was found in two Japanese families A and B, and the same deletion (subtype 2 in Fig. 5) was shared by three Japanese and one Caucasian families D–F, despite apparent nonconsanguinity. This may be explained by assuming that patients with severe phenotype were preferentially examined in the previous studies, whereas those with the AEXS phenotype were analyzed in this study without ascertainment bias. Furthermore, because phenotypes are milder in the duplication and the deletion types than in the inversion type, this may have permitted the spread of the duplication and the deletion types, but not the inversion type, as the founder abnormalities. This notion predicts that the duplication and the deletion types would be identified by examining patients with mild AEXS phenotype.

In summary, the present study shows that AEXS can be caused by duplications of the physiological promoters and microdeletions of the upstream regions of *CYP19A1* and that phenotypic severity is primarily determined by the tissue expression pattern of *CYP19A1* and the chimeric genes and by structural properties of the fused exons. Most importantly, the present study provides novel models for the gain-of-function mutations leading to human genetic disease.

Acknowledgments

Address all correspondence and requests for reprints to: Dr. Tsutomu Ogata, Department of Molecular Endocrinology, National Research Institute for Child Health and Development, 2-10-1 Ohkura, Setagaya, Tokyo 157-8535, Japan. E-mail: tomogata@nch.go.jp.

Present address for T.O.: Department of Pediatrics, Hamamatsu University School of Medicine, Hamamatsu 431-3192, Japan.

This work was supported by Grants for Research on Intractable Diseases (H22-035 and H22-098) from the Ministry of Health, Labor, and Welfare; Grants-in-Aid for Scientific Research (B) (20390265) and (S) (22227002) from the Japan Society for the Promotion of Science; and Grant-in-Aid for Scientific Research on Innovative Areas (22132004) from the Ministry of Education, Culture, Sports, Science, and Technology.

Disclosure Summary: The authors have nothing to declare.

References

1. Bhasin S 2008 Testicular disorders. In: Kronenberg HM, Melmed M, Polonsky KS, Larsen PR, eds. *Williams textbook of endocrinology*. 11th ed. Philadelphia: Saunders; 645–699
2. Bulun SE, Takayama K, Suzuki T, Sasano H, Yilmaz B, Sebastian S

2004 Organization of the human aromatase p450 (CYP19) gene. *Semin Reprod Med* 22:5–9

- Demura M, Reierstad S, Innes JE, Bulun SE 2008 Novel promoter I. 8 and promoter usage in the CYP19 (aromatase) gene. *Reprod Sci* 15:1044–1053
- Harada N, Utsumi T, Takagi Y 1993 Tissue-specific expression of the human aromatase cytochrome P-450 gene by alternative use of multiple exons 1 and promoters, and switching of tissue-specific exons 1 in carcinogenesis. *Proc Natl Acad Sci USA* 90:11312–11316
- Shozu M, Sebastian S, Takayama K, Hsu WT, Schultz RA, Neely K, Bryant M, Bulun SE 2003 Estrogen excess associated with novel gain-of-function mutations affecting the aromatase gene. *N Engl J Med* 348:1855–1865
- Binder G, Iliev DI, Dufke A, Wabitsch M, Schweizer R, Ranke MB, Schmidt M 2005 Dominant transmission of prepubertal gynecomastia due to serum estrone excess: hormonal, biochemical, and genetic analysis in a large kindred. *J Clin Endocrinol Metab* 90:484–492
- Martin RM, Lin CJ, Nishi MY, Billerbeck AE, Latronico AC, Russell DW, Mendonca BB 2003 Familial hyperestrogenism in both sexes: clinical, hormonal, and molecular studies of two siblings. *J Clin Endocrinol Metab* 88:3027–3034
- Demura M, Martin RM, Shozu M, Sebastian S, Takayama K, Hsu WT, Schultz RA, Neely K, Bryant M, Mendonca BB, Hanaki K, Kanzaki S, Rhoads DB, Misra M, Bulun SE 2007 Regional rearrangements in chromosome 15q21 cause formation of cryptic promoters for the CYP19 (aromatase) gene. *Hum Mol Genet* 16:2529–2541
- Tiulpakov A, Kalintchenko N, Semitcheva T, Polyakov A, Dedov I, Sverdlova P, Kolesnikova G, Peterkova V, Rubtsov P 2005 A potential rearrangement between CYP19 and TRPM7 genes on chromosome 15q21.2 as a cause of aromatase excess syndrome. *J Clin Endocrinol Metab* 90:4184–4190
- Stratakis CA, Vottero A, Brodie A, Kirschner LS, DeAtkine D, Lu Q, Yue W, Mitsiades CS, Flor AW, Chrousos GP 1998 The aromatase excess syndrome is associated with feminization of both sexes and autosomal dominant transmission of aberrant P450 aromatase gene transcription. *J Clin Endocrinol Metab* 83:1348–1357
- Bellino FL, Osawa Y 1977 Localization of estrogen synthetase in the chorionic villus fraction after homogenization of human term placenta. *J Clin Endocrinol Metab* 44:699–707
- Kuzniak HA, Maquat LE 2006 Applying nonsense-mediated mRNA decay research to the clinic: progress and challenges. *Trends Mol Med* 12:306–316
- Gu W, Zhang F, Lupski JR 2008 Mechanisms for human genomic rearrangements. *Pathogenetics* 1:4
- Castillo-Davis CI, Mekhedov SL, Hartl DL, Koonin EV, Kondrashov FA 2002 Selection for short introns in highly expressed genes. *Nat Genet* 31:415–418
- Shaw ND, Histed SN, Srouji SS, Yang J, Lee H, Hall JE 2010 Estrogen negative feedback on gonadotropin secretion: evidence for a direct pituitary effect in women. *J Clin Endocrinol Metab* 95:1955–1961
- Belgorosky A, Guercio G, Pepe C, Saraco N, Rivarola MA 2009 Genetic and clinical spectrum of aromatase deficiency in infancy, childhood and adolescence. *Horm Res* 72:321–330
- Alexander DC, Miller WL 1982 Regulation of ovine follicle-stimulating hormone β -chain mRNA by 17 β -estradiol *in vivo* and *in vitro*. *J Biol Chem* 257:2282–2286
- Mercer JE, Clements JA, Funder JW, Clarke IJ 1988 Luteinizing hormone- β mRNA levels are regulated primarily by gonadotropin-releasing hormone and not by negative estrogen feedback on the pituitary. *Neuroendocrinology* 47:563–566
- Raven G, de Jong FH, Kaufman JM, de Ronde W 2006 In men, peripheral estradiol levels directly reflect the action of estrogens at the hypothalamo-pituitary level to inhibit gonadotropin secretion. *J Clin Endocrinol Metab* 91:3324–3328
- Moger WH 1980 Direct effects of estrogens on the endocrine function of the mammalian testis. *Can J Physiol Pharmacol* 58:1011–1022
- Strauss L, Kallio J, Desai N, Pakarinen P, Miettinen T, Gylling H, Albrecht M, Mäkelä S, Mayerhofer A, Poutanen M 2009 Increased exposure to estrogens disturbs maturation, steroidogenesis, and cholesterol homeostasis via estrogen receptor α in adult mouse Leydig cells. *Endocrinology* 150:2865–2872
- Kumar TR, Wang Y, Lu N, Matzuk MM 1997 Follicle stimulating hormone is required for ovarian follicle maturation but not male fertility. *Nat Genet* 15:201–204
- Tapanainen JS, Aittomäki K, Min J, Vaskivuo T, Huhtaniemi IT 1997 Men homozygous for an inactivating mutation of the follicle-stimulating hormone (FSH) receptor gene present variable suppression of spermatogenesis and fertility. *Nat Genet* 15:205–206
- Layman LC, McDonough PG 2000 Mutations of follicle stimulating hormone- β and its receptor in human and mouse: genotype/phenotype. *Mol Cell Endocrinol* 161:9–17

Insulin-Like Growth Factor I Enhances the Expression of Aromatase P450 by Inhibiting Autophagy

Bo Zhang, Makio Shozu, Masahiko Okada, Hiroshi Ishikawa, Tadayuki Kasai, Kouich Murakami, Kazuhito Nomura, Nobuhiro Harada, and Masaki Inoue

Department of Obstetrics and Gynecology (B.Z., M.O., T.K., K.M., K.N., M.I.), Kanazawa University Graduate School of Medicine, Kanazawa 920-0934, Japan; Reproductive Medicine (M.S., H.I.), Graduate School of Chiba University, Chiba 260-8670, Japan; and Department of Biochemistry (N.H.), School of Medicine, Fujita Health University, Toyoake, Aichi 470-1192, Japan

Aromatase, a key enzyme of estrogen biosynthesis, is transcriptionally regulated by many growth factors. IGF-I enhances aromatase activity in a variety of cells, but the mechanism of action has not been determined. We herein report our finding of a novel mechanism of action for IGF-I. IGF-I enhanced the dexamethasone (DEX)-induced aromatase activity by 30% in serum-starved THP-1 cells. The increase was associated with a corresponding increase in the level of aromatase protein but not with any change in the mRNA level. Metabolic labeling experiments revealed that IGF-I inhibited the degradation of aromatase. We identified pepstatin A as the most effective inhibitor of aromatase degradation by *in vitro* assay. Using a nontoxic concentration of pepstatin A, we examined IGF-I's action on aromatase distribution in microsomes and lysosomes. In the presence of pepstatin A, DEX caused an increase in the amount of aromatase in both microsomes and lysosomes, and IGF-I attenuated the DEX-induced accumulation of aromatase in lysosomes and, conversely, enhanced its accumulation in the microsomes. The addition of serum abolished the IGF-I-induced changes. The transport from microsome to lysosome was fluorescently traced in cells using a recombinant aromatase. IGF-I selectively reduced the aromatase signal in the lysosomes. Finally, we observed that IGF-I enhanced the aromatase activity by 50% as early as 1 h after treatment; furthermore, rapamycin, an enhancer of autophagy, completely negated the effect of IGF-I on the enzyme. These results indicate that IGF-I enhances aromatase by the inhibition of autophagy. (*Endocrinology* 151: 4949–4958, 2010)

Aromatase, a member of the P450 superfamily, is a key enzyme of estrogen biosynthesis and catalyzes the conversion of androgen to estrogen. Aromatase is expressed in the gonads, placenta, and other extraglandular tissues including adipose, breast, skin, brain, bone, arterial wall, liver, and uterus. All of these extraglandular tissues are estrogen receptor positive, and estrogen synthesized *in situ* is supposed to work directly on cells in a juxtacrine fashion. Currently, there is growing evidence that dysregulated expression of aromatase in these extraglandular tissues has pathological relevance and that targeting aromatase is an effective strategy for treatment of hormone-dependent tumors arising from these tissues,

i.e. breast cancer, endometriosis, and leiomyoma of the uterus (1–5).

To understand the mechanisms responsible for the localized dysregulation (overexpression) of aromatase, researchers, including the authors of this paper, have extensively studied and found that a variety of tumor-derived humoral factors play pivotal roles in the localized induction of aromatase. For example, in breast cancer, malignant epithelial cells secrete significant quantities of prostaglandin E2, which induces transcription of aromatase in stromal cells surrounding breast cancer cells via the most proximal promoters of aromatase (promoter I.3 and PII) (6). Cytokines such as IL-6, oncostatin M, IL-11, TNF α ,

ISSN Print 0013-7227 ISSN Online 1945-7170

Printed in U.S.A.

Copyright © 2010 by The Endocrine Society

doi: 10.1210/en.2010-0294 Received March 11, 2010. Accepted June 29, 2010.

First Published Online July 28, 2010

Abbreviations: DEX, Dexamethasone; FBS, fetal bovine serum; GAPDH, glyceraldehyde-3-phosphate dehydrogenase; mTOR, mammalian target of rapamycin; PMSF, phenylmethylsulfonyl fluoride; RIPA, radioimmunoprecipitation assay.

and IL-1 β stimulate aromatase transcription in stromal cells via a distal aromatase promoter (promoter I.4) (7–11) in the presence of circulating levels of glucocorticoids, which play a permissive role for the transcription (12). In addition to the transcriptional activation, TNF α and IL-11 can also enhance aromatase in breast cancer tissues by inhibiting the differentiation of aromatase-positive adipose stromal cells into aromatase-negative mature adipocytes (13).

IGF-I, a potent signaling molecule whose signaling pathway is implicated in the development and progression of a number of human neoplasms, including breast cancers (14), is also known to enhance aromatase. The precise mechanism is, however, still the subject of investigation. Unlike other factors that act in a cell- and promoter-specific fashion as described above, IGF-I consistently enhances aromatase in different types of cells (granulosa lutein cells, adipose stromal cells, skin fibroblasts, breast cells and breast cancer cells, and Leydig tumor cells) that use different types of aromatase promoters (15–19). Transcriptional activation through the induction of steroidogenic factor-1, a key transcription factor for the PII promoter, and indirect actions through the acceleration of follicular development and granulosa cell proliferation have been proposed as mechanisms of IGF-I's action in Leydig cells and granulosa cells, respectively (18, 20–22). These mechanisms explain the PII promoter-induced enhancement of aromatase in these cells but do not explain how IGF-I enhances aromatase in such a wide variety of cells that use different types of promoters.

We herein uncovered a novel mechanism whereby IGF-I enhances aromatase in a variety of cells, namely inhibition of autophagy. This action may explain the non-selective enhancement of ectopic expression of aromatase by IGF-I and its role in many human pathologies, including polycystic ovary syndrome and endometrial cancer, where free IGF-I and insulin are both high in serum (23, 24). This may also indicate the therapeutic relevance of a new class of anticancer drugs targeting mammalian target of rapamycin (mTOR), a gatekeeper of autophagy as well as cell proliferation (*i.e.* the use of an mTOR inhibitor may interfere with aromatase *in situ*).

Materials and Methods

Chemicals

IGF-I was purchased from R&D Systems (Minneapolis, MN). Dexamethasone (DEX) and all other chemicals, unless specifically indicated, were purchased from Sigma Chemical Co. (St. Louis, MO).

Cell culture

THP-1 (a human acute monocytic leukemia cell line) and JEG-3 cells (a human placental choriocarcinoma cell line) were purchased from the American Type Culture Collection (Rockville, MD) and cultured as described. For serum starvation, THP-1 cells were maintained for 6–24 h in RPMI 1640 medium supplemented with 0.1% BSA (albumin solution from fraction V from bovines; Sigma). The intrinsic aromatase-negative KW cells, previously established from an aromatase-positive myometrial cell line, were used for transfection experiments to trace extrinsic aromatase without interference from intrinsic aromatase (25–27).

Aromatase activity

Serum-starved THP-1 cells and KW cells were treated with IGF-I (5 ng/ml), DEX (2.5 nM), or both for 15 min to 48 h in RPMI 1640 medium supplemented with 0.1% BSA and 1 β -[3 H]androstenedione (final concentration 60 nM; NEN Life Science Products, Boston, MA) was added to the medium 1 h before the end of incubation, unless otherwise specified. The aromatase activity was assayed by formation of tritiated water from 1 β -[3 H]androstenedione as previously described (12, 28). The aromatase activity was expressed as the rate of formation of tritiated water per milligram of protein corresponding to 2 h of incubation.

Western blot

Western blotting was conducted as described previously (27). The polyclonal anti-aromatase antibody was obtained from the serum of rabbits immunized with placenta-derived aromatase (29). The antibody for P450 cytochrome oxidoreductase (CYPOR) was purchased from Santa Cruz Biotechnology (sc-25263; Santa Cruz, CA) and used to assure even loading of microsomal protein. The protein concentrations were determined by the bicinchoninic acid method (BCA Protein Assay Reagent, Pierce, Rockford, IL).

Quantification of aromatase mRNA

The aromatase P450 mRNA was measured by real-time PCR using primer pairs designed to amplify the exon 2–4 sequences as described previously (30). We also quantified the promoter-specific transcript levels of aromatase by exon-1-specific competitive RT-PCR using internal standard RNA as described previously (27, 31).

Aromatase expression vectors and transient transfection

The full-length aromatase cDNA was amplified from the pCMV-aromatase expression vector (pCMV-arom) (32) by PCR and was subcloned into the pcDNA3.1D/V5-His vector (pcDNA3.1D/V5-arom), in which a 14-amino-acid V5 epitope was added on the C-terminal end of the aromatase cDNA (pcDNA3.1 Directional TOPO expression kit; Invitrogen, Carlsbad, CA). The fidelity of the sequence was confirmed by sequencing.

Expression vectors were transiently transfected into KW cells using Superfect Reagent (QIAGEN, Valencia, CA) as described elsewhere (30, 33). The aromatase activity of the pCMV-arom- and pcDNA3.1D/V5-arom-transfected KW cells was examined by the tritiated water formation assay as described above.

Preparation of subcellular fractions

The cellular fractions of THP-1 cells were prepared by sequential centrifugations as described elsewhere (27). Briefly, cells were lysed on ice with buffer A [10 mM PBS, 15 mM KCl, 1 mM EDTA (pH 6.88)] and subsequently sonicated on ice. The lysate was centrifuged 10 min at 800 \times g to remove nuclei, 10 min at 5000 \times g to remove mitochondria, and 10 min at 10,000 \times g to recover lysosomes as precipitates. The lysosome-rich precipitates were washed one time and solubilized using a modified radioimmunoprecipitation assay (RIPA) buffer [5 mM Tris, 1 mM EDTA, 1% Nonidet P-40 (pH 7.5)]. The supernatant was again centrifuged for 60 min at 105,000 \times g to recover microsomes (27). The pellets were washed one time and resuspended in 50 μ l buffer containing 50 mM PBS, 20% glycerol, 1 mM EDTA, and 1 mM dithiothreitol. Both microsomal and cytosolic fractions were snap-frozen in liquid nitrogen and stored at –80°C until use.

Placental tissues were obtained from patients, who gave the consent for the study, after normal delivery. The institutional review board approved this study. The placental tissues were homogenized, and microsome fractions were similarly prepared and stored at –80°C until use.

For detection of cellular aromatase, microsomal fractions were used for Western blotting. For detection of aromatase in the lysosome, crude lysosome fractions were refined by density-gradient centrifugation (lysosome enrichment kit; Pierce) to assure the subcellular localization.

35 S metabolic labeling experiments

THP-1 cells were pretreated with DEX (2.5 nM) in serum-free medium for 24 h. For pulse-labeling experiments, the cells were preincubated for 60 min in DMEM without methionine and cysteine supplemented with 0.1% BSA and were then pulse labeled for 60 min with 50 μ Ci/ml of Pro-Mix L- 35 S *in vitro* cell labeling mix (GE Healthcare, Buckinghamshire, UK). 35 S-labeled cells were rinsed twice with PBS and incubated with regular RPMI 1640 culture medium (with 0.1% BSA) supplemented with cold methionine and cysteine (0.2 mM L-cysteine HCl, 2 mM L-glutamine) with or without IGF-I (5 ng/ml). The cells were lysed with 1 ml modified RIPA buffer. The lysates were centrifuged at 10,000 \times g for 10 min at 4°C, and the supernatants were used as the whole-cell extract. To remove any nonspecific proteins, 100 μ l extract was gently mixed with 20 μ l recombinant protein A agarose beads (protein A-Sepharose 4B conjugate; Invitrogen) and then incubated for 1 h at 4°C. The mixture was thereafter briefly centrifuged to remove the agarose beads; 0.5 μ l rabbit polyclonal antihuman aromatase antibody, anti- β -actin antibody, and anti-glyceraldehyde-3-phosphate dehydrogenase (GAPDH) antibody were added to the supernatant; and the reaction was allowed to proceed with incubation at 4°C overnight with continuous agitation. After incubation, 20 μ l agarose beads was added, and incubation was resumed for 1 h. The sample was centrifuged at 5000 \times g for 1 min and the antigen-antibody complex-bound beads were saved and washed five times with modified RIPA buffer. The washed beads were suspended with 10 μ l 2 \times SDS-PAGE sample buffer [125 mM Tris-HCl (pH 6.8), 10% 2-mercaptoethanol, 10% SDS, 10% glycerol] and boiled for 5 min. The extracted proteins were separated on a 10% SDS-polyacrylamide gel. Gels were dried and developed using the BAS 2000 system (Fujifilm, Tokyo, Japan). Radioactivity was expressed as the percentage of that at time zero.

In vitro degradation assay

The degradation of aromatase was assessed by the *in vitro* coincubation with fractionated cell lysates as a source of degradation enzymes. Placental microsomal fractions (1–5 μ g protein) as a measure of crude aromatase were incubated with an aliquot of solubilized cellular fractions (1.0 μ g whole-cell homogenates, lysosome fraction, or cytosol fraction), prepared from JEG-3 cells or THP-1 cells. After an 8-h incubation at room temperature, residual aromatase protein was detected by Western blotting. Preliminary experiments showed that degradation proceeded most efficiently using a lysosomal fraction prepared from JEG-3 cells. The lysosome fractions were thus used for *in vitro* degradation assay.

Placental aromatase was stable in neutral to mild acidic conditions (pH 7.4–7.0) for at least 8 h at room temperature and was degraded by coincubation with lysosomal fractions in acidic conditions (pH \leq 7.0). Degradation occurred more rapidly as the pH became more acidic, and acidic hydrolysis (a nonenzymatic mechanism resulting in degradation) became prominent under extremely acidic conditions (pH \sim 4.0). Therefore, the following experiments were conducted at pH 5.3 to minimize the contribution of nonenzymatic hydrolysis and maximize enzymatic digestion.

To identify the most effective inhibitors of degradation, the above assay was conducted in the presence of several type of inhibitors, including pepstatin A (an aspartate protease inhibitor), 3,4-dichloroisocoumarin (a serine protease inhibitor), E64 (a cysteine protease inhibitor), aprotinin (a serine protease inhibitor), phenylmethylsulfonyl fluoride (PMSF, a serine protease inhibitor), sodium fluoride (an esterase inhibitor), sodium metavanadate (a phosphatase inhibitor), and MG132 (a proteasome inhibitor).

Detection of aromatase in subcellular fractions

The serum-starved THP-1 cells were treated with DEX (2.5 nM), IGF-I (5 ng/ml), or both for 24 h in serum-free medium. Six hours before the end of the incubation, 0.1 mg/ml pepstatin A was added to the medium. The lysosomal and microsomal fractions were prepared and purified as described above in the presence of protease inhibitors (1 mM PMSF, 1 μ g/ml aprotinin, and 1 μ g/ml pepstatin A). The lysosomal fractions (0.3 μ g protein per lane) and microsomal fractions (0.25 μ g protein per lane) were then examined for aromatase expression by Western blotting.

Immunofluorescence staining

KW cells were grown on coverslips for 24 h and transiently transfected with pcDNA3.1D/arom-V5 plasmid (0.05 μ g DNA per well of six-well plates) with 0.45 μ g pUC19 DNA. After a 16-h recovery in complete medium containing 10% fetal bovine serum (FBS), the cells were fed with serum-free medium supplemented with 0.1% BSA for 6 h and thereafter with fresh serum-free medium containing IGF-I (5 ng/ml) for the last 24 h. Pepstatin A (0.1 mg/ml) and Lysotracker Red DND-99 (50 μ M; Invitrogen), and ER-Tracker RED (glibenclamide BODIPY TR; Invitrogen) were added to the medium 6 and 1 h before the end of the incubation, respectively. Aromatase was stained using an anti-V5-fluorescein isothiocyanate antibody (Invitrogen). Briefly, the cells on the coverslips were fixed in 100% methanol for 5 min at room temperature and then subsequently with 1% BSA/PBS for blocking and finally were incubated with anti-V5-fluorescein isothiocyanate antibody diluted to 1:500 (Invitrogen). The cells

were imaged with an Olympus BX51 epifluorescence microscope. The images were captured with a charge-coupled device camera and the OpenLab software program (Nippon Roper, Tokyo, Japan) using a constant exposure time for each filter combination. Composite images were colored and assembled with Adobe Photoshop 5.5 (Adobe Systems, Mountain View, CA) with no alterations in the relative gray scale levels.

The aromatizing ability was confirmed by tritiated water released from 1β -[3 H]androstenedione in pcDNA3.1D/arom-V5-transfected KW cells.

Statistical analysis

Data are expressed as the means \pm SEM unless otherwise specified. Differences in the transcription level and activity between the two groups were evaluated using the Mann-Whitney *U* test for unpaired data and Wilcoxon signed rank test for paired data. Statistical significance was established at the $P < 0.05$ level.

Results

IGF-I enhances aromatase activity without increasing the mRNA level

The aromatase activity of serum-starved THP-1 cells was measured in the presence or absence of IGF-I. IGF-I alone increased the basal level of aromatase activity by roughly 30% after 24 h of treatment (Fig. 1A). IGF-I similarly enhanced the DEX-induced level of aromatase activity by 30% (Fig. 1A). When the activity was assessed in the presence of DEX, the enhancement was significant at 12 and 24 h of IGF-I stimulation but was no longer significant by 48 h after initiation of treatment (Fig. 1B).

To clarify the mechanism by which IGF-I increases aromatase activity, the level of aromatase protein was quantitated by Western blot analysis at 24 h. IGF-I increased the amount of aromatase protein by 30% in the presence of DEX, which corresponded to the increase in its activity (Fig. 1C). To determine whether the increase in protein was due to increased transcription, the mRNA level of aromatase was subsequently measured by real-time RT-PCR. In contrast to the protein level, the mRNA level of aromatase did not show any increase in response to IGF-I, either in the presence or absence of DEX (Fig. 1D). The absence of any transcriptional influence of IGF-I was also confirmed by promoter-specific RT-PCR for aromatase.

This lack of effect on aromatase transcription was confirmed using KW cells, which were transiently transfected with pCMV-aromatase. IGF-I enhanced the aromatase activity without inducing a significant increase in aromatase transcription from the cytomegalovirus promoter-driven promoter (Fig. 1, E and F).

IGF-I stabilizes the aromatase protein

The coordinated increase in the protein and activity levels of aromatase (without a corresponding increase in

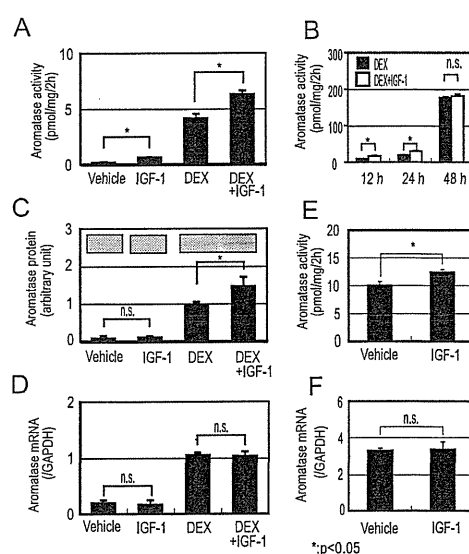


FIG. 1. The effect of IGF-I on the expression of aromatase in THP-1 cells. A, C, and D, The effect of 24 h IGF-I treatment on the activity (A), protein level (C), and coding mRNA level (D) of aromatase. Each bar represents the mean \pm SEM of the values obtained from five independent experiments conducted in triplicate wells. The microsomal fraction was prepared by sequential ultracentrifugation and used for Western blot analysis. Inset images were taken from the same film. The amount of aromatase-coding mRNA was expressed as the ratio to GAPDH mRNA. Data represent the mean \pm SEM of four independent experiments. B, The time course of the effects of IGF-I on aromatase activity. Data represent the mean \pm SEM of four independent experiments. E and F, Effect of IGF-I on aromatase activity (E) and aromatase mRNA expression (F) in KW cells expressing pCMV-arom. After the recovery in complete medium for 12 h, transfected cells were starved for 6 h and then treated with IGF-I (5 ng/ml) for 20 h. Data were obtained from five independent experiments.

the transcript level) suggested that IGF-I exerts its effects via a posttranscriptional mechanism. To confirm this hypothesis, the degradation of the aromatase protein was assessed by a 35 S metabolic labeling experiment. As shown in Fig. 2, A and B, IGF-I reduced the turnover of aromatase as early as 2 h after the initiation of treatment, and this effect continued for at least 6 h. GAPDH, a microsomal enzyme that is a target of chaperone-mediated autophagy, was similarly immunoprecipitated, and a degradation curve was produced for comparison purposes (Fig. 2C). The degradation curve of GAPDH was similar to that of aromatase under normal conditions, but IGF-I had no effect on GAPDH degradation.

Aromatase degradation is sensitive to pepstatin A

To determine the proteases responsible for aromatase degradation, we conducted an *in vitro* degradation assay and sought the most effective protease inhibitor(s). Pepstatin A efficiently inhibited aromatase degradation, whereas 3,4-dichloroisocoumarin, E64, aprotinin, and PMSF did not. The inhibitory actions of sodium fluoride and sodium metavanadate were suboptimal. These results suggest that

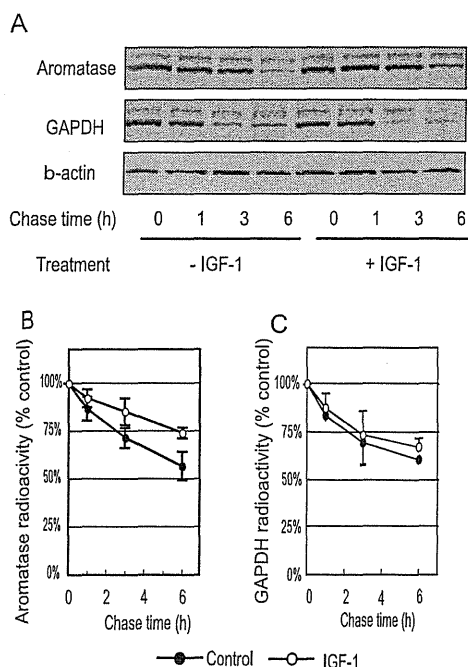


FIG. 2. Effect of IGF-I on the degradation rate of pulse-labeled aromatase protein in THP-1 cells. A, A representative autoradiogram of immunoprecipitated proteins; B and C, time course of radioactivity of aromatase and GAPDH obtained from four independent experiments.

lysosomal cathepsin families, such as cathepsin D (which is sensitive to pepstatin A), are primarily involved in the degradation of aromatase.

IGF-I reduces DEX-dependent accumulation of aromatase in lysosomes

We thereafter determined the *in vivo* effect of IGF-I in the presence of pepstatin A, a cell membrane-permeable inhibitor. A concentration of 0.1 mg/ml pepstatin A in the culture medium did not result in any toxicity to the THP-1 cells according to a morphological assessment; furthermore, it did not affect the cell number or lactic dehydrogenase activity. We initially thought that this nontoxic concentration of pepstatin A would enhance aromatase, but it did not increase either the activity or the protein level in the microsomal fraction (Supplemental Fig. 1, published on The Endocrine Society's Journals Online web site at <http://endo.endojournals.org>).

We subsequently compared the subcellular localization of aromatase. Immunogenic aromatase (54 kDa) was barely detectable in lysosomal fractions under normal conditions (Fig. 3A). However, in the presence of pepstatin A, DEX alone caused a profound increase in the expression of immunogenic aromatase (54 kDa) in the lysosomal fraction, whereas IGF-I attenuated the DEX-induced accumulation of lysosomal aromatase (Fig. 3B). Conversely, IGF-I enhanced the DEX-induced accumulation of immunogenic aromatase in the microsomal fraction.

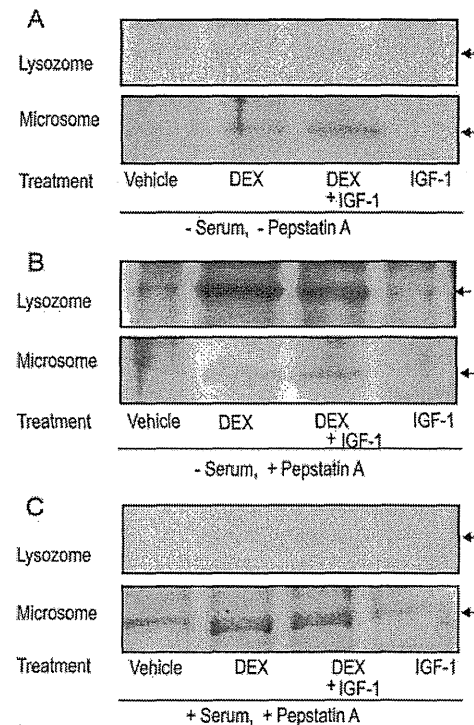


FIG. 3. The subcellular localization of aromatase in the presence of pepstatin A. Cellular fractions were prepared from THP-1 cells incubated with vehicle alone (A), pepstatin A (B), or pepstatin A plus 10% FBS (C). The arrows indicate the size of the placental microsome that run in the same gel.

tion (Fig. 3, A and B, *second vs. third line*). This reciprocal action of IGF-I in the lysosomal and microsomal fractions suggests that DEX simultaneously increases the synthesis of aromatase and also increases the transport of the newly synthesized aromatase into lysosomes; furthermore, IGF-I inhibits this transport of aromatase into lysosomes and consequently enhances the accumulation of aromatase in the microsomes.

The addition of serum markedly reduced the levels of aromatase in the lysosomal fractions and enhanced the aromatase level in microsomal fractions (Fig. 3C). Furthermore, the addition of serum completely abolished the IGF-I-induced changes in the aromatase levels by enhancing the concentration in the microsomal fractions and attenuating the expression in the lysosomal fractions.

IGF-I inhibits the lysosomal transport of aromatase

Subcellular transport of aromatase was morphologically traced using KW cells that expressed pcDNA3.1D/V5-arom. V5-tagged aromatase was localized in the endoplasmic reticulum (Fig. 4, A–C). After 24 h of treatment with IGF-I, the color of the lysosomes changed to a reddish orange (Fig. 4I) from a yellowish orange in the merged figures (Fig. 4F), indicating that IGF-I reduced the concentration of aromatase in the lysosomes. An IGF-I-induced color change of the lysosome was observed even in

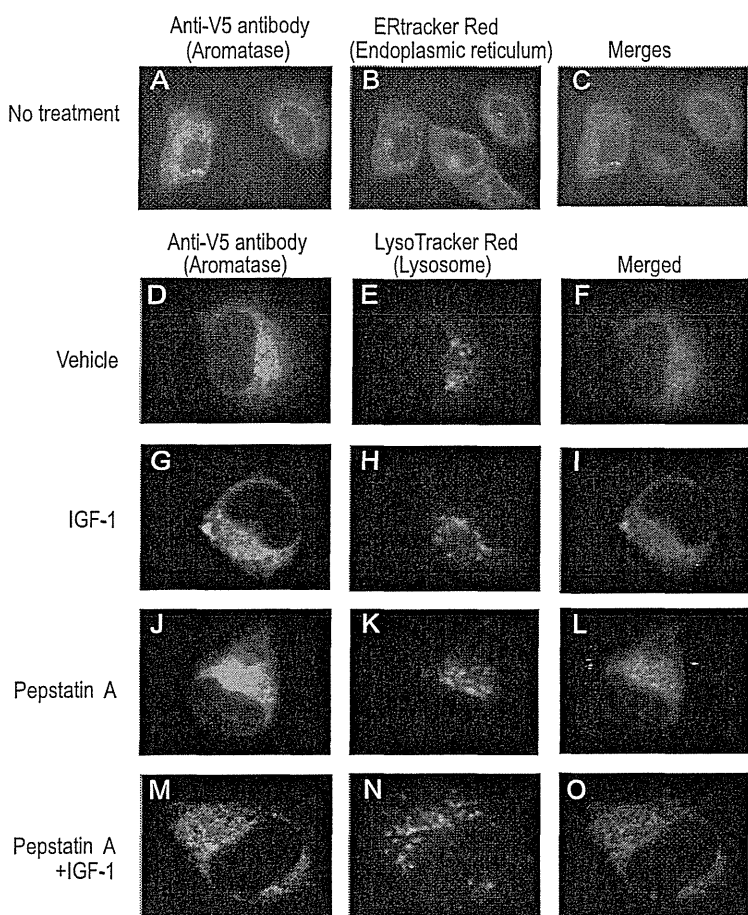


FIG. 4. Fluorescent detection of the subcellular localization of the recombinant aromatase in KW cells. A, Antibodies against His tag of aromatase; B, ER-Tracker RED for endoplasmic reticulum; C, a merged image of A and B; D–O, aromatase (D, G, J, and M) was stained green, and lysosomes were stained red (E, H, K, and N). KW cells were cultured in the presence of vehicle only (D–F), IGF-I (5 ng/ml, G–I), pepstatin A (0.1 mg/ml, J–L), or pepstatin A plus IGF-I (M–O). A representative figure is shown for each treatment. Note that the exogenous aromatase was overexpressed in the transfected KW cells without DEX, despite lower dilutions of the vector. Thus, it might be possible to suppose that autophagy occurred in these cells without DEX.

the presence of pepstatin A (Fig. 4, O vs. L). As shown in Fig. 4L, pepstatin A alone induced no or a minimal change in the lysosomal color. The results after a 1-h treatment with IGF-I were essentially the same, thus demonstrating that the activity occurs rapidly after treatment with IGF-I. These findings are consistent with the notion that IGF-I inhibits the transport of aromatase into lysosomes and that pepstatin A inhibits the degradation of aromatase in lysosomes.

The action of IGF-I on aromatase activity is rapid, rapamycin dependent, and serum starvation dependent

Based on the results reported above, we hypothesized that IGF-I enhances aromatase activity by inhibiting autophagy. To support this hypothesis, we performed two complementary experiments.

To show that the enhancement in expression and activity by IGF-I is a rapid process, THP-1 cells, which were preincubated with DEX in serum-free medium to induce aromatase, were challenged with IGF-I in serum-free medium, and the aromatase activity was measured every 15 min. As expected, the aromatase activity decreased in a time-dependent fashion (Fig. 5A). IGF-I overcame the reduction in aromatase and reversed the trend, resulting in an increase in expression by approximately 50% *vs.* a time-matched control as early as 60 min after the initiation of treatment. The increase in activity observed with IGF-I treatment was most likely due to the temporal continuation of protein synthesis from preexisting mRNA in the absence of protein degradation after the removal of DEX. Conversely, the rate of protein degradation probably exceeded the rate of protein synthesis in the control groups, thus resulting in the rapid decrease in activity over time. Therefore, IGF-I's action on aromatase is a rapid process, comparable to the rapid regulation of the autophagic process through the sequential activation of the kinase cascade (34, 35).

We next examined the effect of inhibiting autophagy on the expression and activity of aromatase. The addition of 1% serum and 1% ethanol eliminated the acute IGF-I-induced increase in aromatase activity at 60 min (data not shown). Similarly, the addition of rapamycin, which directly inhibits mTOR and induces autophagy, abolished the IGF-I-induced enhancement of aromatase activity at 60 min after treatment (Fig. 5B).

Discussion

Aromatase is a short-lived protein, and its expression is regulated primarily at the transcriptional level (12, 36–39). Regulation through protein phosphorylation and degradation by the proteasome have also been reported (37, 39–42). The present study demonstrated a previously unknown mechanism of aromatase regulation, namely autophagy. Autophagy down-regulated aromatase, and conversely, the inhibition of autophagy by IGF-I caused an acute and profound increase in aromatase activity. This autophagy-dependent mechanism well explains the serum dependence of the effects of IGF-I, and does demonstrate the importance of the serum concentration in culture medium for the measurement of aromatase activity in cell-based assays.

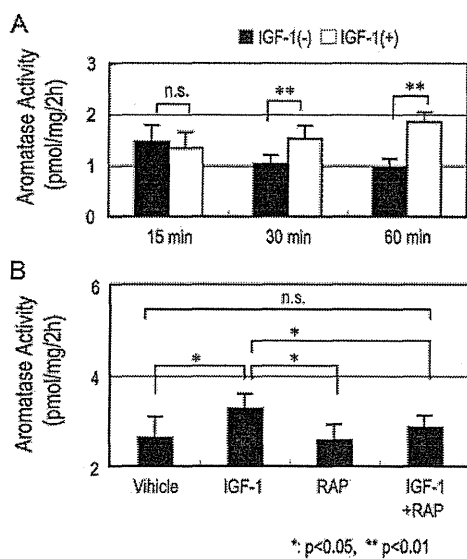


FIG. 5. Acute effects of IGF-I and rapamycin on aromatase activity. **A**, THP-1 cells were maintained to fully induce aromatase for 42 h in complete medium containing 10% FBS and 25 nm DEX. After 6 h of starvation in serum-free medium containing 25 nm DEX, the cells were washed three times with PBS and fed with serum-free and DEX-free medium containing IGF-I (5 ng/ml). Aromatase activity was measured by every 15-min incubation with 1β -[3 H]androstenedione. Data are presented as the mean \pm SEM of four independent experiments. **B**, THP-1 cells were pretreated as above and were challenged with IGF-I (5 ng/ml), rapamycin (1 μ g/ml), or both for 60 min. Aromatase activity was determined by a 15-min incubation with 1β -[3 H]androstenedione at the end of the culture. Data are from five independent experiments.

It has previously been reported that the addition of serum in culture media potentiates the expression of aromatase in many different cell types (12, 28, 43). This action has been ascribed to the effects of serum-derived factors on the transcription of the protein (9, 15). In fact, several humoral factors (including cytokines, growth factors, prostaglandins, and some hormones) in the serum activate aromatase promoters and therefore activate its transcription. In addition to transcriptional up-regulation, our results revealed the contribution of the proteolytic process to the acute control of aromatase activity. Increased aromatase activity was also observed after the addition of albumin to serum-starved breast cancer cells in the mid 1990s, but the underlying mechanism of this phenomenon had never been determined (15, 44). The suppression of autophagy by albumin would, at least in part, explain the enhancement of aromatase activity. In fact, it has already been shown by the same author that IGF-I increases the cellular uptake of iodo-labeled albumin (44). Ethanol also increases the basal activity of aromatase, and transcriptional up-regulation by ethanol has been reported in breast cancer cells (45). This enhancement of aromatase activity could also be attributed, at least in part, to autophagy, because ethanol suppresses autophagy (46).

Our Western blot analysis of cellular fractions demonstrated that IGF-I reduced aromatase in the lysosomes and

concurrently increased aromatase in the microsomes (Fig. 3B). In concert with the change in the aromatase activity, the addition of serum completely abrogated the IGF-I-induced changes in aromatase expression levels seen in the lysosomes and microsomes (Fig. 3C). This close coupling between microsomal and lysosomal aromatase supports the notion that IGF-I enhances the functional aromatase residing in microsomes by inhibiting its translocation into lysosomes. This type of subcellular translocation can occur through autophagy.

Autophagy is a degradation pathway for the disposal of cellular components, by which eukaryotic cells can renew their own components and restore the metabolic balance during conditions of nutrient starvation. There are three major mechanisms for autophagy: chaperone-mediated autophagy (degradation of specific cytosolic proteins), macroautophagy (bulk degradation of cytosol and organelles), and microautophagy (engulfing portions of cytosolic material and organelles) (47). Autophagy is induced by amino acid deficiency and is inhibited by IGF-I through the activation of mTOR kinase complexes (34, 35). Serum abolished the aromatase-enhancing activity of IGF-I in THP-1 cells. Rapamycin, an inhibitor of mTOR, also repressed the IGF-I-induced enhancement of aromatase activity, thus supporting the role of autophagy. The effect of IGF-I on aromatase is observed in nearly all types of aromatase-expressing cells that were examined under serum-free conditions, including the intrinsic aromatase-negative KW cells that were transfected to express aromatase driven by a viral promoter. This suggests that the mechanism for disposing of aromatase was not specifically developed for aromatase-expressing cells. The kinetics of aromatase degradation shown by our pulse-chase experiment were different from that of GAPDH, a well known target of chaperone-mediated autophagy (48, 49). Collectively, these results are consistent with the notion that autophagy, specifically macroautophagy, is the mechanism responsible for the translocation of aromatase. We are currently using electron microscopic analysis to directly assess the process of macroautophagy under these conditions.

During macroautophagy, a small double-membrane structure is initially induced in the cytosol. This structure subsequently expands around and sequesters an organelle to form an autophagosome. The autophagosome eventually fuses with the lysosomal membrane, thus allowing the contents to be digested (in the autophagolysosome) (47). The lysosomal fraction that we prepared by density gradient centrifugation included both autophagosomes and autophagolysosomes (50, 51), whereas the microsome fraction contained the endoplasmic reticulum, where aromatase resides as a functional protein. Therefore, the re-

duction in lysosomal aromatase signifies that IGF-I inhibited the step before the completion of autophagosome formation, thus keeping enzymes active. In contrast, pepstatin A prevented just the final step of autophagy, leading to conservation of the aromatase protein in the autophagolysosome, which had already been sequestered from substrates in the cytosol, so that the protein would no longer function. This explains why IGF-I, but not pepstatin A, enhanced aromatase activity in cells, whereas both suppressed autophagy.

To confirm the effect of IGF-I on autophagy, we conducted a morphological examination using KW cells that expressed cytomegalovirus promoter-driven aromatase. KW cells are derived from myometrial smooth muscle cells that express low basal levels and high induced levels of aromatase under pathological conditions, such as the generation of a leiomyoma. KW cells, despite being aromatase negative, are therefore potentially equipped with a system to express and dispose of aromatase, and this system would be affected by IGF-I in the same way as cells with higher basal expression levels. We used the KW cells to examine the fate of recombinant aromatase, without the potential interference of endogenous aromatase. Our results demonstrated that IGF-I reduced the aromatase signal within the lysosomes, even in the presence of pepstatin A (Fig. 4, L vs. O). The use of pepstatin A, an inhibitor of lysosomal proteases, would intensify the aromatase signal within the lysosomes if formation of aromatase-containing autophagolysosomes continued in the presence of IGF-I. Our observation that this did not occur indicates that the formation of aromatase-engulfing autophagosomes had been virtually stopped by treatment with IGF-I.

DEX induced an increase in lysosomal aromatase regardless of whether IGF-I existed (Fig. 3B, compare the second lane to the first lane and the third lane to the fourth lane to observe the action of DEX in the absence and presence of IGF-I, respectively). When there is increased protein synthesis, more mis- or unfolded proteins accumulate as more new protein is formed, and this dysfunctional protein is tracked into the lysosome for disposal (34). Because DEX strongly induces aromatase transcription (12), it is reasonable to assume that DEX activates the transcription (and therefore the translation) of aromatase, which consequently increases the number of dysfunctional aromatase molecules translocated into the lysosomes. Under conditions of relative malnutrition, there may be more chances of mis-incorporation of amino acids and therefore much production of dysfunctional aromatase protein. However, this quality-control mechanism may not fully explain all of the DEX-induced increase in the amount of aromatase in lysosomal fractions. When the cells were treated with IGF-I, it led to the preservation of the DEX-

induced aromatase that had been synthesized during the malnutrition, and this enzyme was still functional. This means that even normally folded, and thus functional, protein had been routed into the lysosomes under serum-free conditions. Based on these findings, we reasoned that DEX induces autophagy in nutrient-poor cells, which consequently reduces the amount of aromatase protein. Our preliminary experiment using electron microscopy demonstrated that autophagosome is increased in DEX-treated THP-1 cells. Recently, similar DEX-induced autophagy was reported for the mouse lymphoma cell line WEHI7.2 (52, 53). Therefore, DEX appears to have a dual action on aromatase activity in serum-starved THP-1 cells; it increases the aromatase activity by transcriptional activation and decreases its activity by enhancing autophagy.

It is interesting to note that the rapid control observed in our study, including the down-regulation by autophagy, may play an important role in the brain, where rapid changes in estrogen action through rapid changes in aromatase activity occur in physiologically relevant situations (54). Such activity may also be important in the ovary, where rapid control of aromatase activity may be responsible for rapid fluctuations in the serum estradiol concentration (55). However, the precise pathophysiological significance remains to be determined. New drugs targeting the mTOR complex, a gatekeeper for cell proliferation, apoptosis, and autophagy, are currently being developed for various types of cancer, including breast, colon, and esophageal cancer. Because aromatase is overexpressed in all of these cancers, it is expected that these mTOR inhibitors may be especially effective. It may also be worthwhile to consider the potential modification of aromatase when these drugs are examined in clinical trials.

In summary, we have demonstrated that IGF-I enhances aromatase activity by inhibiting the induction of autophagy in serum-starved cells treated with DEX. This finding reveals a novel mechanism for the rapid and profound clearance of aromatase activity. Moreover, our findings emphasize the need to pay attention to the nutritional condition of cells when aromatase expression is experimentally assessed.

Acknowledgments

Address all correspondence and requests for reprints to: Prof. Makio Shozu, Department of Reproductive Medicine, Graduate School of Medicine, Chiba University, 1-8-1 Inohana, Chuoh-ku, Chiba 260-8670, Japan. E-mail: shozu@faculty.chiba-u.jp.

This study was supported by a Grant-in-Aid for Scientific Research (A) 16209049 and a Grant-in-Aid for Exploratory Research No. 20659257 from the Japanese Ministry of Education, Culture, Sports, Science, and Technology and by the Megumi Medical Foundation, Kanazawa, Japan.

Disclosure Summary: None of the authors have anything to disclose.

References

1. Santen RJ, Brodie H, Simpson ER, Siiteri PK, Brodie A 2009 History of aromatase: saga of an important biological mediator and therapeutic target. *Endocr Rev* 30:343–375
2. Bulun SE, Imir G, Utsunomiya H, Thung S, Gurates B, Tamura M, Lin Z 2005 Aromatase in endometriosis and uterine leiomyomata. *J Steroid Biochem Mol Biol* 95:57–62
3. Shozu M, Murakami K, Inoue M 2004 Aromatase and leiomyoma of the uterus. *Semin Reprod Med* 22:51–60
4. Shipp ER, West Jr WJ 2004 Successful treatment of severe endometriosis in two premenopausal women with an aromatase inhibitor. *Fertil Steril* 81:1395–1398
5. Shozu M, Murakami K, Segawa T, Kasai T, Inoue M 2003 Successful treatment of symptomatic uterine leiomyoma with a nonsteroidal aromatase inhibitor in a perimenopausal woman. *Fertil Steril* 79: 628–631
6. Bulun SE, Lin Z, Zhao H, Lu M, Amin S, Reierstad S, Chen D 2009 Regulation of aromatase expression in breast cancer tissue. *Ann NY Acad Sci* 1155:121–131
7. Zhao Y, Mendelson CR, Simpson ER 1995 Characterization of the sequences of the human CYP19 (aromatase) gene that mediate regulation by glucocorticoids in adipose stromal cells and fetal hepatocytes. *Mol Endocrinol* 9:340–349
8. Zhao Y, Nichols JE, Valdez R, Mendelson CR, Simpson ER 1996 Tumor necrosis factor- α stimulates aromatase gene expression in human adipose stromal cells through use of an activating protein-1 binding site upstream of promoter 1.4. *Mol Endocrinol* 10:1350–1357
9. Zhao Y, Nichols JE, Bulun SE, Mendelson CR, Simpson ER 1995 Aromatase P450 gene expression in human adipose tissue. Role of a Jak/STAT pathway in regulation of the adipose-specific promoter. *J Biol Chem* 270:16449–16457
10. Shozu M, Zhao Y, Simpson ER 2000 TGF- β 1 stimulates expression of the aromatase (CYP19) gene in human osteoblast-like cells and THP-1 cells. *Mol Cell Endocrinol* 160:123–133
11. Shozu M, Sumitani H, Segawa T, Yang HJ, Murakami K, Kasai T, Inoue M 2002 Overexpression of aromatase P-450 in leiomyoma tissues is driven through the promoter I. 4 of aromatase P-450. *J Clin Endocrinol Metab* 87:2540–2548
12. Shozu M, Zhao Y, Simpson ER 1997 Estrogen biosynthesis in THP1 cells is regulated by promoter switching of the aromatase (CYP19) gene. *Endocrinology* 138:5125–5135
13. Meng L, Zhou J, Sasano H, Suzuki T, Zeitoun KM, Bulun SE 2001 Tumor necrosis factor α and interleukin 11 secreted by malignant breast epithelial cells inhibit adipocyte differentiation by selectively down-regulating CCAAT/enhancer binding protein α and peroxisome proliferator-activated receptor γ : mechanism of desmoplastic reaction. *Cancer Res* 61:2250–2255
14. Pollak MN, Schernhammer ES, Hankinson SE 2004 Insulin-like growth factors and neoplasia. *Nat Rev Cancer* 4:505–518
15. Reed MJ, Topping L, Coldham NG, Purohit A, Ghilchik MW, James VH 1993 Control of aromatase activity in breast cancer cells: the role of cytokines and growth factors. *J Steroid Biochem Mol Biol* 44:589–596
16. Steinkampf MP, Mendelson CR, Simpson ER 1988 Effects of epidermal growth factor and insulin-like growth factor I on the levels of mRNA encoding aromatase cytochrome P-450 of human ovarian granulosa cells. *Mol Cell Endocrinol* 59:93–99
17. Emoto N, Ling N, Baird A 1991 Growth factor-mediated regulation of aromatase activity in human skin fibroblasts. *Proc Soc Exp Biol Med* 196:351–358
18. Chabrolle C, Tosca L, Ramé C, Lecomte P, Royère D, Dupont J 2009 Adiponectin increases insulin-like growth factor I-induced progesterone and estradiol secretion in human granulosa cells. *Fertil Steril* 92:1988–1996
19. Randolph Jr JF, Kipersztok S, Ayers JW, Ansbacher R, Peegel H, Menon KM 1987 The effect of insulin on aromatase activity in isolated human endometrial glands and stroma. *Am J Obstet Gynecol* 157:1534–1539
20. Sirianni R, Chimento A, Malivindi R, Mazzitelli I, Andò S, Pezzi V 2007 Insulin-like growth factor-I, regulating aromatase expression through steroidogenic factor 1, supports estrogen-dependent tumor Leydig cell proliferation. *Cancer Res* 67:8368–8377
21. Ginther OJ, Bergfelt DR, Beg MA, Meira C, Kot K 2004 In vivo effects of an intrafollicular injection of insulin-like growth factor 1 on the mechanism of follicle deviation in heifers and mares. *Biol Reprod* 70:99–105
22. Spicer LJ, Chamberlain CS, Maciel SM 2002 Influence of gonadotropins on insulin- and insulin-like growth factor-I (IGF-I)-induced steroid production by bovine granulosa cells. *Domest Anim Endocrinol* 22:237–254
23. Thierry van Dessel HJ, Lee PD, Faessen G, Fauser BC, Giudice LC 1999 Elevated serum levels of free insulin-like growth factor I in polycystic ovary syndrome. *J Clin Endocrinol Metab* 84:3030–3035
24. Ayabe T, Tsutsumi O, Sakai H, Yoshikawa H, Yano T, Kurimoto F, Taketani Y 1997 Increased circulating levels of insulin-like growth factor-I and decreased circulating levels of insulin-like growth factor binding protein-1 in postmenopausal women with endometrial cancer. *Endocr J* 44:419–424
25. Matsuo O, Fukao H, Izaki S, Matsuo C, Ueshima S 1989 Production and characterization of single-chain tissue-type plasminogen activator produced by an established cell line from human uterine muscle. *Cell Struct Funct* 14:45–60
26. Sourla A, Reyes-Moreno C, Koutsilieris M 1994 Characterization of KW smooth muscle-like human myometrial cells. *Anticancer Research* 14:1887–1892
27. Sumitani H, Shozu M, Segawa T, Murakami K, Yang HJ, Shimada K, Inoue M 2000 *In situ* estrogen synthesized by aromatase P450 in uterine leiomyoma cells promotes cell growth probably via an autocrine/intracrine mechanism. *Endocrinology* 141:3852–3861
28. Shozu M, Simpson ER 1998 Aromatase expression of human osteoblast-like cells. *Mol Cell Endocrinol* 139:117–129
29. Harada N 1988 Novel properties of human placental aromatase as cytochrome P-450: purification and characterization of a unique form of aromatase. *J Biochem* 103:106–113
30. Ishikawa H, Shozu M, Okada M, Inukai M, Zhang B, Kato K, Kasai T, Inoue M 2007 Early growth response gene-1 plays a pivotal role in down-regulation of a cohort of genes in uterine leiomyoma. *J Mol Endocrinol* 39:333–341
31. Shozu M, Zhao Y, Bulun SE, Simpson ER 1998 Multiple splicing events involved in regulation of human aromatase expression by a novel promoter, I. 6. *Endocrinology* 139:1610–1617
32. Corbin CJ, Graham-Lorence S, McPhaul M, Mason JI, Mendelson CR, Simpson ER 1988 Isolation of a full-length cDNA insert encoding human aromatase system cytochrome P-450 and its expression in nonsteroidogenic cells. *Proc Natl Acad Sci USA* 85:8948–8952
33. Shozu M, Murakami K, Segawa T, Kasai T, Ishikawa H, Shinohara K, Okada M, Inoue M 2004 Decreased expression of early growth response-1 and its role in uterine leiomyoma growth. *Cancer Res* 64:4677–4684
34. Klionsky DJ, Emr SD 2000 Autophagy as a regulated pathway of cellular degradation. *Science* 290:1717–1721
35. Young AR, Narita M, Ferreira M, Kirschner K, Sadaie M, Darot JF, Tavaré S, Arakawa S, Shimizu S, Watt FM, Narita M 2009 Autophagy mediates the mitotic senescence transition. *Genes Dev* 23: 798–803
36. Bulun SE, Sebastian S, Takayama K, Suzuki T, Sasano H, Shozu M 2003 The human CYP19 (aromatase P450) gene: update on phys-

iologic roles and genomic organization of promoters. *J Steroid Biochem Mol Biol* 86:219–224

37. Shozu M, Sumitani H, Murakami K, Segawa T, Yang HJ, Inoue M 2001 Regulation of aromatase activity in bone-derived cells: possible role of mitogen-activated protein kinase. *J Steroid Biochem Mol Biol* 79:61–65
38. Chen S, Ye J, Kijima I, Kinoshita Y, Zhou D 2005 Positive and negative transcriptional regulation of aromatase expression in human breast cancer tissue. *J Steroid Biochem Mol Biol* 95:17–23
39. Catalano S, Barone I, Giordano C, Rizza P, Qi H, Gu G, Malivindi R, Bonofiglio D, Andò S 2009 Rapid estradiol/ER α signaling enhances aromatase enzymatic activity in breast cancer cells. *Mol Endocrinol* 23:1634–1645
40. Balthazart J, Baillien M, Charlier TD, Cornil CA, Ball GF 2003 Multiple mechanisms control brain aromatase activity at the genomic and non-genomic level. *J Steroid Biochem Mol Biol* 86:367–379
41. Wang X, Chen S 2006 Aromatase destabilizer: novel action of exemestane, a food and drug administration-approved aromatase inhibitor. *Cancer Res* 66:10281–10286
42. Miller TW, Shin I, Kagawa N, Evans DB, Waterman MR, Arteaga CL 2008 Aromatase is phosphorylated in situ at serine-118. *J Steroid Biochem Mol Biol* 112:95–101
43. Lanoux MJ, Cleland WH, Mendelson CR, Carr BR, Simpson ER 1985 Factors affecting the conversion of androstenedione to estrogens by human fetal hepatocytes in monolayer culture. *Endocrinology* 117:361–368
44. Singh A, Blench I, Morris HR, Savoy LA, Reed MJ 1992 Synergistic interaction of growth factors and albumin in regulating estradiol synthesis in breast cancer cells. *Mol Cell Endocrinol* 85:165–173
45. Etique N, Chardard D, Chesnel A, Merlin JL, Flament S, Grillier-Vuissoz I 2004 Ethanol stimulates proliferation, ER α and aromatase expression in MCF-7 human breast cancer cells. *Int J Mol Med* 13:149–155
46. Donohue Jr TM 2009 Autophagy and ethanol-induced liver injury. *World J Gastroenterol* 15:1178–1185
47. Todde V, Veenhuis M, van der Klei IJ 2009 Autophagy: principles and significance in health and disease. *Biochim Biophys Acta* 1792:3–13
48. Franch HA, Soopar S, Du J, Brown NS 2001 A mechanism regulating proteolysis of specific proteins during renal tubular cell growth. *J Biol Chem* 276:19126–19131
49. Shen W, Brown NS, Finn PF, Dice JF, Franch HA 2006 Akt and Mammalian target of rapamycin regulate separate systems of proteolysis in renal tubular cells. *J Am Soc Nephrol* 17:2414–2423
50. Nixon RA, Wegiel J, Kumar A, Yu WH, Peterhoff C, Cataldo A, Cuervo AM 2005 Extensive involvement of autophagy in Alzheimer disease: an immuno-electron microscopy study. *J Neuropathol Exp Neurol* 64:113–122
51. Singh R, Kaushik S, Wang Y, Xiang Y, Novak I, Komatsu M, Tanaka K, Cuervo AM, Czaja MJ 2009 Autophagy regulates lipid metabolism. *Nature* 458:1131–1135
52. Swerdlow S, McColl K, Rong Y, Lam M, Gupta A, Distelhorst CW 2008 Apoptosis inhibition by Bcl-2 gives way to autophagy in glucocorticoid-treated lymphocytes. *Autophagy* 4:612–620
53. Laane E, Tamm KP, Buentke E, Ito K, Kharazia P, Khahariza P, Oscarsson J, Corcoran M, Björklund AC, Hultenby K, Lundin J, Heyman M, Söderhäll S, Mazur J, Porwit A, Pandolfi PP, Zhivotovskiy B, Panaretakis T, Grandér D 2009 Cell death induced by dexamethasone in lymphoid leukemia is mediated through initiation of autophagy. *Cell Death Differ* 16:1018–1029
54. Cornil CA, Ball GF, Balthazart J 2006 Functional significance of the rapid regulation of brain estrogen action: where do the estrogens come from? *Brain Res* 1126:2–26
55. Lephart ED, Simpson ER, McPhaul MJ 1992 Ovarian aromatase cytochrome P-450 mRNA levels correlate with enzyme activity and serum estradiol levels in anestrous, pregnant and lactating rats. *Mol Cell Endocrinol* 85:205–214



Earn more than 100 hours of CME credit through
ENDO 2010 Session Library.

<http://www.endo-society.org/endo>

特集

子宮内膜症合併不妊の治療法

[各論] 妊孕性向上のための内膜症治療

10. 子宮内膜症治療と アロマターゼ阻害剤

しょう す ま せ る う す い ひろ かず
生水真紀夫*・碓井宏和*

千葉大学大学院医学研究院生殖機能病態学*

提
要

子宮内膜症組織にはアロマターゼが過剰に発現しており、局所で産生されるエストロゲンが内膜症の発育・進展に関与している可能性がある。アロマターゼ阻害剤による内膜症治療は、この局所アロマターゼを標的分子としている。単独もしくは黄体ホルモン剤やGnRHアゴニスト等との併用投与で、疼痛の軽減に有効である可能性が示唆されている。妊娠性の改善効果については不明である。

Key Words aromatase inhibitor, endometriosis

子宮内膜症は黄体ホルモン受容体陽性であり、従来から黄体ホルモン剤が治療に用いられてきた。子宮内膜症はエストロゲン受容体も陽性であり、エストロゲン依存性の発育を示すことから、エストロゲンもまた治療標的となっている。GnRHアゴニストは、卵巣からのエストロゲン分泌を低下させる目的で使用されている。黄体ホルモン剤やダナゾールにもゴナドトロピン抑制作用があり、治療効果の少なくとも一部は、卵巣性エストロゲンの低下による。

この 10 年ほどの間の研究から、子宮内膜症組織自体がエストロゲン合成酵素であるアロマターゼを発現しており、血中のアンドロゲンを原料として組織内でエストロゲンを産生していることが明らかとなった。

この内膜症組織内で産生されたエストロゲンが内膜症細胞自身の増殖を促し、その病態形成

に関与している可能性があり、局所のアロマターゼを内膜症治療の標的とする臨床研究も行われている。本稿では、アロマターゼ阻害剤による治療の理論的背景とこれまでの臨床報告を概説する。

子宮内膜症組織における アロマターゼの発現

子宮内膜症組織では、おもに間質細胞でアロマターゼが過剰に発現しており、エストロゲンが過剰に産生されている(図 1)。このエストロゲンは、内膜上皮に作用して増殖を促進するとともに、シクロオキシゲナーゼ 2 型酵素(cyclooxygenase type 2, COX2)の発現を誘導しプロスタグランジン E2 等の産生を促す。プロスタグランジン E2 は炎症性反応のメディエーターとなり、内膜症病変の進行や疼痛の発生を

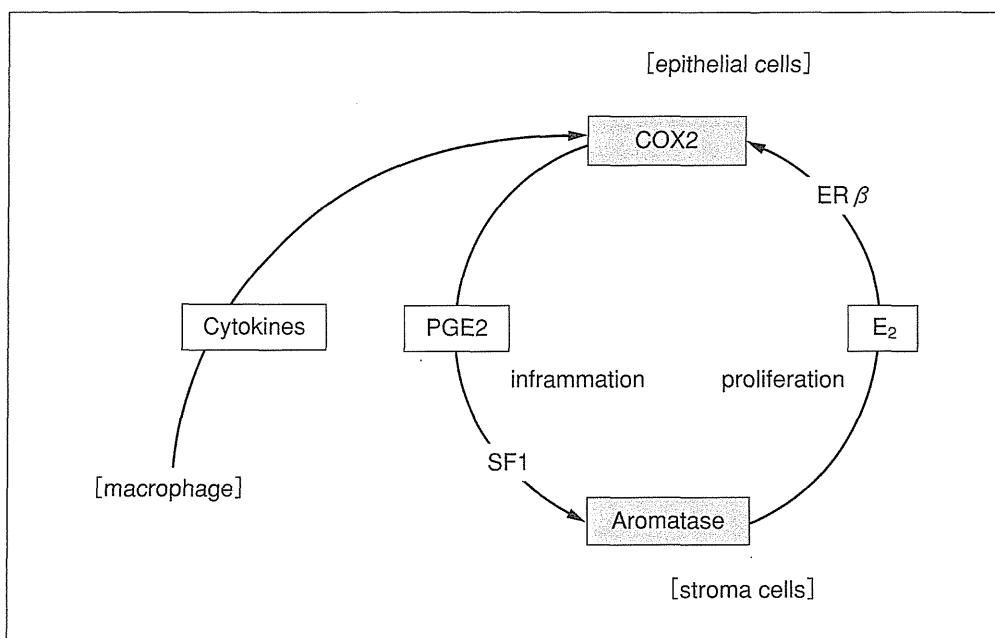


図1 内膜症組織におけるエストロゲンとプロスタグランジン産生系と内膜症進展への寄与
(positive feed forward loop)

PGE2: プロスタグランジン E2, E₂: エストラジオール

促進する。さらに、プロスタグランジン E2 には、間質細胞のアロマターゼ発現を誘導する作用がある。亢進したアロマターゼはエストロゲンを産生し、エストロゲンがさらに COX2 の発現を促進する。すなわち、間質のアロマターゼと上皮の COX2 が positive feed forward loop を作っていて、それぞれの生産物であるエストロゲンとプロスタグランジン E2 を介して、内膜症の増殖・進展に関わると推測される。

ゲノムの脱メチル化やメチル化などのエピゲノム変化が、子宮内膜症におけるアロマターゼとその発現調節因子、特に steroidogenic factor 1 の発現亢進に関わっているとの推測がある¹⁾。しかし、ゲノムの脱メチル化などのエピゲノム変化は、炎症性メディエーターが長期に作用した結果である可能性もあり、アロマターゼ発現異常の真の原因はよくわかっていない。

阻害剤の作用機序

アロマターゼ阻害剤の治療効果は、内膜症組織内のエストロゲンレベルの低下によってもたらされると考えられる。

アロマターゼ阻害剤が卵巣のアロマターゼを抑制する可能性はあるが、有経者に通常量を投与した場合にもたらされる血中エストラジオール濃度の低下はほんのわずかで、投与前値とほとんど変わらないかもしくは 1/2~1/5 程度の低下と考えられる^{2)~4)}(アロマターゼ阻害剤の投与量は、閉経後乳癌患者を対象にして設定されている。すなわち、卵巣周期の閉止した女性で乳癌局所でのエストロゲン産生が低下する投与量に設定されている)。したがって、卵巣におけるエストロゲン産生の低下が、治療効果の本体とは考えにくい。

これに対して、子宮内膜症組織内でのエストロゲン産生は、アロマターゼ阻害剤によりほぼ